

Retardation effects and the Coulomb pseudopotential in the theory of superconductivity

Johannes Bauer,^{1,2} Jong E. Han,^{1,3} and Olle Gunnarsson¹

¹*Max Planck Institute for Solid State Research, Heisenbergstr.1, D-70569 Stuttgart, Germany*

²*Department of Physics, Harvard University, Cambridge, Massachusetts 02138, USA and*

³*Department of Physics, SUNY at Buffalo, Buffalo, New York 14260, USA*

(Dated: June 26, 2018)

In the theory of electron-phonon superconductivity both the magnitude of the electron-phonon coupling λ as well as the Coulomb pseudopotential μ^* are important to determine the transition temperature T_c and other properties. We calculate corrections to the conventional result for the Coulomb pseudopotential. Our calculation are based on the Hubbard-Holstein model, where electron-electron and electron-phonon interactions are local. We develop a perturbation expansion, which accounts for the important renormalization effects for the electrons, the phonons, and the electron-phonon vertex. We show that retardation effects are still operative for higher order corrections, but less efficient due to a reduction of the effective bandwidth. This can lead to larger values of the pseudopotential and reduced values of T_c . The conclusions from the perturbative calculations are corroborated up to intermediate couplings by comparison with non-perturbative dynamical mean-field results.

PACS numbers: 71.10.Fd, 71.27.+a, 71.30.+h, 75.20.-g, 71.10.Ay

I. INTRODUCTION

More than a century after its discovery superconductivity continues to be subject of intense research in condensed matter physics. The research ranges from topics geared to the technical application of the phenomenon over the search for new superconducting materials to fundamental questions of microscopic mechanisms.¹ The latter are important as one might hope that a good understanding of the mechanisms will make the design of new superconductors at elevated temperatures feasible.^{2,3} There are numerous classes of materials for which different mechanisms are discussed.^{1,4} In most cases a bosonic pairing function is invoked, which could be of purely electronic origin such as spin fluctuations, or the conventional phonon mechanism, but also more exotic mechanisms have been proposed. The electron-phonon mechanism has the longest history and probably the most established mathematical foundation. An effective electron-electron attraction generated by the electron-phonon interaction is part of the celebrated Bardeen-Cooper-Schrieffer (BCS) theory.⁵ The more elaborate theory including microscopic details goes under the name Migdal-Eliashberg (ME) theory.⁶ With the help of ME theory the superconducting properties of many elements and numerous alloys have been described accurately.^{7,8}

The general ideas of ME theory can be presented in relatively simple fashion, although the details of the complete framework, its foundations and specific applications, involve a substantial degree of sophistication to which many researcher have contributed over the years.⁷⁻¹⁰ One cornerstone is Migdal's theorem,¹¹ which employs the fact that the typical electronic energy scale E_{el} and the typical phonon energy scale ω_{ph} differ largely, such that E_{el}/ω_{ph} is of the order 100 and larger - the electrons move much faster than the phonons. It can then be shown that the perturbation theory of the electron-

phonon problem greatly simplifies since vertex corrections are small. The influence of the bosonic pairing function $\alpha^2F(\omega)$ on the electronic properties and the occurrence of superconductivity can therefore be computed reliably. A remarkable aspect of the ME theory is that it is even well justified for large values of the electron-phonon coupling parameter $\lambda > 1$ as long as the effective expansion parameter $\sim \lambda\omega_{ph}/E_{el}$ remains small.¹¹⁻¹³ With the help of the ME equations, the pairing function $\alpha^2F(\omega)$ and the phenomenological parameter for the Coulomb pseudopotential μ^* were extracted from tunneling measurement in a procedure termed inverse tunneling spectroscopy.¹⁴ Based on those other properties such as T_c or thermodynamic quantities can be computed. The agreement with the respective experimental values of many elements and alloys, notably Pb and Nb, is within the range of a few percent.⁷ This leads to a consistent picture and was taken as proof of the validity of ME theory and the electron-phonon mechanism.^{7,8} Further support comes from first principle calculations for $\alpha^2F(\omega)$, which are in many cases in remarkable agreement with the results extracted from tunneling.^{7,8,15,16}

In addition to the effective attraction induced by the electron-phonon coupling the applications of ME theory include the effects of the Coulomb repulsion. Due to the enormous success of the theory it is sometimes understated that in contrast to the electron-phonon problem no rigorous arguments exist for the treatment of the Coulomb repulsion,¹⁰ the reason being the absence of a small parameter as in Migdal's theorem. Traditionally, this is seen as minor deficiency based on the following arguments. Some effects of the Coulomb interaction, such as the renormalization of the electron-phonon couplings, g , the electron and phonon dispersion $\varepsilon_{\mathbf{k}}, \omega_{\mathbf{q}}$ are implicit in the experimentally derived results or in the first principle calculations. It remains to deal with the direct repulsion in the pairing channel which opposes s-wave super-

conductivity. Morel and Anderson proposed a procedure in two stages:¹⁷ first the Coulomb interaction is screened and averaged over the Fermi surface. In a second step it is projected to the phonon scale. The result possesses the famous form,^{9,17,18}

$$\mu_c^* = \frac{\mu_c}{1 + \mu_c \log\left(\frac{E_{\text{el}}}{\omega_{\text{ph}}}\right)}, \quad (1)$$

which is sometimes termed the Morel-Anderson (MA) pseudopotential. Here, μ_c is a dimensionless quantity which consists of a product of the the averaged, screened Coulomb interaction with the density of states per spin at the Fermi energy; E_{el} is an electronic scale, such as the half bandwidth D or the Fermi energy E_{F} , and ω_{ph} the phonon scale, e.g. the Debye frequency. Eq. (1) has the important property that for the typical large energy separation between electronic and phonon scale, $E_{\text{el}} \gg \omega_{\text{ph}}$, such that $\log(E_{\text{el}}/\omega_{\text{ph}}) \sim 5 - 10$, μ_c^* is much smaller than μ_c . This effect is remarkable, as it enables the electron-phonon s-wave superconductivity to be possible in spite of the Coulomb repulsion, which on a bare level is much larger and working directly against it. This is sometimes even termed the true mechanism of electron-phonon superconductivity.⁸ The textbook physical picture is that electrons do not need to be close in position space and suffer from the Coulomb repulsion in order to pair since the electron-phonon interaction is retarded and thus electrons can pair with a “time-delay”. Using appropriate energy scales in Eq. (1) leads to estimates of the order $\mu_c^* \sim 0.1 - 0.14$. This fits well to the parameters μ^* obtained from tunneling in many elemental superconductors and alloys.⁷ Hence, the Coulomb effects are generally considered to be well described by μ^* , which is a fairly universal quantity. In contrast to the pairing function it is usually not calculated based on first principles and rather used as a fitting parameter. It is worth mentioning that there is also an alternative ab-initio approach to superconductivity based on the DFT framework.¹⁹⁻²¹

Review of the literature however also reveals evidence that the description of the Coulomb repulsion in the form of Eq. (1) is incomplete. In some cases, such as V or Nb₃Ge,⁷ the values for μ^* appear to be of the order 0.2 – 0.3 substantially larger than the traditional quotes, even though the maximal phonon scales does not seem to be particularly large. Density functional theory (DFT) calculation¹⁶ for $\alpha^2 F(\omega)$ find good agreement with the tunneling results, but to explain the experimental values for T_c also somewhat larger values of μ^* have to be used. A specific case which raises doubts about the conventional framework is the example of elemental lithium at ambient pressure.^{22,23} The coupling constant was estimated to be $\lambda \sim 0.4$,^{22,24} which seems to be in line with specific heat measurements. With the usual value of $\mu^* \sim 0.1$ and the appropriate phonon scale this implies $T_c \sim 1\text{K}$. This is in contrast to experiments where for a long time no superconductivity was observed down to values of 6mK,²⁵ and only recently, $T_c \sim 0.4\text{mK}$ was found at ambient pressure, which requires $\mu^* \sim 0.23$.²⁶ In this

context, we also mention alkali doped picene, which was recently discovered to be superconducting at $T_c \sim 7\text{K}$ and $T_c \sim 18\text{K}$ depending on preparation.²⁷ First principle calculations only seem to be able to explain these values of T_c based on an electron-phonon mechanism with relatively large values of $\mu^* \sim 0.23$.²⁸ However, also other interpretations exist.^{29,30}

It is our endeavor to reanalyze the expression for the Coulomb pseudopotential in Eq. (1) and calculate corrections to it. We focus on the reduction of phonon induced s-wave superconductivity due to the Coulomb repulsion between electrons. Superconductivity which is induced in an anisotropic higher order angular momentum channel by purely repulsive interactions, such as the well-known Kohn-Luttinger effect³¹, is not dealt with in the present work. Berk and Schrieffer³² included a specific class of higher order diagrams describing the coupling to ferromagnetic (FM) spin fluctuations, addressing almost FM metals, like Pd. They found that retardation is ineffective for the added diagrams and that superconductivity is strongly suppressed, which can help to explain the cases when FM spin fluctuations are important. In another line of work going beyond MA the jellium model for electrons was considered and the Eliashberg equation were solved including the frequency and momentum dependence of the dynamically screened Coulomb interaction. Curiously, random phase approximation (RPA) calculations by Rietschel and Sham yielded negative values for μ_c^* when the density parameter r_s exceeded values $r_s > 2.5$.³³ The resulting unrealistic large values for T_c were interpreted as plasmon induced superconductivity.³⁴ It was shown that vertex corrections lead to a reduction of T_c and partly cure this problem.^{34,35} Phenomenological models of the form of Kukkonen and Overhauser³⁶ for the screened Coulomb interaction mostly yield realistic positive results for $\mu_c^* \sim 0.1$ and no s-wave superconductivity,^{23,37} although there also exist different conclusions.³⁸ We remark that Richardson and Ashcroft²³ arrived at a rather accurate prediction for T_c in Li at ambient pressure based on such calculations. Nevertheless, there does not seem to be a conclusive study, which systematically analyzes higher order corrections to the unphysical RPA result.

Rather than treating the Coulomb interaction in the electron gas, our approach is based on a model with local interactions.³⁹ It can thus be interpreted as only considering the second step of the MA procedure, where the projection of the screened interaction to the phonon scale is considered. To be specific we take the Hubbard-Holstein (HH) model, where there is a local electron-electron repulsion and an electron-phonon interaction present. The advantage of the restriction to this model is that it can be analyzed by means of the dynamical mean field theory (DMFT).⁴⁵ Since the DMFT becomes exact in the limit of large dimensions, it can provide benchmark results independent of the interaction strength and thus allows us to test otherwise uncontrolled perturbative approximations. Retardation effects encoded in the frequency de-

pendence of the self-energies are fully contained. DMFT treats both the electron-phonon and the electron-electron interaction non-perturbatively and therefore include contributions to μ_c^* to all orders. However, it also includes renormalization effects of the phonons, the electrons and the electron-phonon coupling. This makes the interpretation of the results and the extraction of μ_c^* more difficult. In order to be able to nevertheless obtain meaningful insights, we developed a diagrammatic perturbative approach for the HH model in the limit of large dimensions. This allows us to see how accurate the conventional theory describes the benchmark results and which corrections are necessary to get a good agreement between the perturbative results and DMFT. We will see that higher order corrections to μ_c^* enter in a modified form when compared to Eq. (1).

The occurrence of superconductivity in the HH model has been analyzed theoretically beyond ME theory.^{40–44} Freericks and Jarrel⁴⁰ studied the suppression of the instabilities towards charge density wave (CDW) formation and superconductivity at and away from half filling within the framework of DMFT. Their finding of robustness of CDW against superconductivity could be explained within weak coupling perturbation theory without invoking corrections to the pseudopotential result in Eq. (1). Functional renormalization group studies^{43,44} found spin density wave (SDW), CDW and different superconducting instabilities. The phonon scale in those works was however relatively large such that retardation effects only played a moderate role.

In this work we show that retardation effects lead to the reduction $\mu_c \rightarrow \mu_c^*$ also in the higher order calculation, but not as efficiently as for the first order one. Non-perturbative DMFT calculations clarify that the perturbative result is accurate up to intermediate coupling strength. An important conclusion is then that retardation effects indeed lead to rather small values of μ_c^* , even when contributions beyond the standard theory are considered. For systems with sizable Coulomb interactions μ_c , our values for μ_c^* are however larger than in the standard theory and therefore lead to reduced values of the superconducting gap and T_c . The paper is structured as follows: In Sec. II, the details of the model are introduced as well as some basic properties of the DMFT approach. In Sec. III, we discuss the diagrammatics for the calculation of T_c from the pairing equation, including self-energy and vertex corrections. In Sec. IV, similar diagrams are discussed for the calculation of the gap at $T = 0$. In Sec. V, we focus on the calculation of the

μ_c^* and derive analytic results including the higher order corrections. In Sec. VI, we put together the results from the perturbation theory and validate our findings up to intermediate couplings with the non-perturbative DMFT results, followed by the conclusions.

II. MODEL AND DMFT SETUP

The purpose of our work is to obtain generic insights into the behavior of a coupled electron-phonon system. Specifically, we employ the Hubbard-Holstein model,

$$H = - \sum_{i,j,\sigma} (t_{ij} c_{i,\sigma}^\dagger c_{j,\sigma} + \text{h.c.}) + U \sum_i \hat{n}_{i,\uparrow} \hat{n}_{i,\downarrow} \quad (2)$$

$$+ \omega_0 \sum_i b_i^\dagger b_i + g \sum_i (b_i + b_i^\dagger) \left(\sum_\sigma \hat{n}_{i,\sigma} - 1 \right).$$

$c_{i,\sigma}^\dagger$ creates an electron at lattice site i with spin σ , and b_i^\dagger a phonon with oscillator frequency ω_0 , $\hat{n}_{i,\sigma} = c_{i,\sigma}^\dagger c_{i,\sigma}$. The electrons interact locally with strength U , and their density is coupled to an optical phonon mode with coupling constant g . The local oscillator displacement is related to the bosonic operators by $\hat{x}_i = (b_i + b_i^\dagger)/\sqrt{2\omega_0}$, where $\hbar = 1$, and one can define a characteristic length $x_0 = 1/\sqrt{\omega_0}$ for the oscillator. We have set the ionic mass to $M = 1$ in (2). The model in Eq. (2) possesses the minimal ingredients necessary, such as energy scales for electrons, phonons and their interactions. In the limit of large dimensions this model can be solved exactly by DMFT. Hence, we can provide controlled benchmark results in this situation. The following calculations are based on this model in the limit of large dimension. In this case the self-energy is independent of the momentum \mathbf{k} , but retains the full frequency dependence. This can be compared with the usual application of ME theory, where one usually projects to the Fermi surface and only deals with frequency dependent quantities.

A. Calculating T_c

In DMFT the critical temperature can be calculated by analyzing the relevant susceptibility. For completeness we display some of the results, which we use later. The notation follows the one in Ref. 45. The equation for the s-wave superconductivity susceptibility $\chi_{\mathbf{q}}(i\omega_n)$ reads with $\chi_{\mathbf{q}}(i\omega_n) = \sum_{n_1, n_2} \tilde{\chi}_{\mathbf{q}}(i\omega_{n_1}, i\omega_{n_2}; i\omega_n)$,

$$\tilde{\chi}_{\mathbf{q}}(i\omega_{n_1}, i\omega_{n_2}; i\omega_n) = \tilde{\chi}_{\mathbf{q}}^0(i\omega_{n_1}, i\omega_{n_2}; i\omega_n) + \frac{1}{\beta} \sum_{n_3, n_4} \tilde{\chi}_{\mathbf{q}}^0(i\omega_{n_1}, i\omega_{n_3}; i\omega_n) \Gamma^{(\text{pp})}(i\omega_{n_3}, i\omega_{n_4}; i\omega_n) \tilde{\chi}_{\mathbf{q}}(i\omega_{n_4}, i\omega_{n_2}; i\omega_n). \quad (3)$$

$\Gamma^{(\text{pp})}(i\omega_{n_1}, i\omega_{n_4}; i\omega_n)$ is the irreducible vertex in the particle-particle channel which is local in DMFT. The

corresponding pair propagator $\tilde{\chi}_{\mathbf{q}}^0(i\omega_{n_1}; i\omega_n)$ is

$$\tilde{\chi}_{\mathbf{q}}^0(i\omega_{n_1}, i\omega_{n_2}; i\omega_n) = \sum_{\mathbf{k}} G_{\mathbf{k}}(i\omega_{n_1}) G_{\mathbf{q}-\mathbf{k}}(i\omega_n - i\omega_{n_1}) \delta_{n_1, n_2}, \quad (4)$$

For special values of \mathbf{q} and $i\omega_n$ we can evaluate the pair propagator.⁴⁵ We are interested in the limit $\mathbf{q} \rightarrow 0$ and $i\omega_n \rightarrow 0$, and one finds

$$\tilde{\chi}_0^0(i\omega_{n_1}, i\omega_{n_2}; 0) = \frac{G(i\omega_{n_1}) - G(-i\omega_{n_1})}{\zeta(-i\omega_{n_1}) - \zeta(i\omega_{n_1})} \delta_{n_1, n_2}, \quad (5)$$

where $\zeta(i\omega_n) = i\omega_n + \mu - \Sigma(i\omega_n)$ and

$$G(i\omega_n) = \int_{-D}^D d\varepsilon \frac{\rho_0}{\zeta(i\omega_n) - \varepsilon} \equiv \text{HT}[\rho_0](\zeta(i\omega_n)). \quad (6)$$

One has for the semi-elliptic DOS

$$\text{HT}[\rho_0](z) = \int_{-D}^D d\varepsilon \frac{\rho_0(\varepsilon)}{z - \varepsilon} = \frac{1}{2t^2} \left(z - \text{sgn}(\text{Im}(z)) \sqrt{z^2 - 4t^2} \right), \quad (7)$$

where the square root of a complex number w is given by $\sqrt{re^{i\varphi/2}}$, where $\varphi = [0, 2\pi)$, such that the imaginary part of \sqrt{w} is positive. At half filling $G(i\omega_n)$ and $\Sigma(i\omega_n)$ are purely imaginary functions. The phonon Green's function $D(i\omega_m)$,

$$D(i\omega_m)^{-1} = D^0(i\omega_m)^{-1} - \Sigma_{\text{ph}}(i\omega_m), \quad (8)$$

where $D^0(i\omega_m) = 2\omega_0/[(i\omega_m)^2 - \omega_0^2]$, and its self-energy $\Sigma_{\text{ph}}(i\omega_m)$ are real functions. In the non-interacting case the Green's function reads,

$$G(i\omega_n) = \frac{i}{2t^2} \left(\omega_n - \text{sgn}(\omega_n) \sqrt{\omega_n^2 + 4t^2} \right). \quad (9)$$

At half filling $\mu = 0$, $G(-i\omega_n) = -G(i\omega_n)$, $\Sigma(-i\omega_n) = -\Sigma(i\omega_n)$. With $\Sigma(i\omega_n) = i\omega_n(1 - Z(i\omega_n))$, where $Z(i\omega_n)$ is symmetric and real, we find

$$\tilde{\chi}_0^0(i\omega_{n_1}, i\omega_{n_2}; 0) = -\frac{G(i\omega_{n_1})}{i\omega_{n_1} Z(i\omega_{n_1})} \delta_{n_1, n_2}. \quad (10)$$

This expression is positive.

We can write Eq. (3) as a matrix equation (omitting the general arguments, $\mathbf{q}, i\omega_n$),

$$\tilde{\chi} = \tilde{\chi}^0 + \tilde{\chi}^0 \Gamma \tilde{\chi}. \quad (11)$$

The instability criterion is that χ diverges for some $T, i\omega_n, \mathbf{q}$. This can be written as the eigenvalue equation $[\tilde{\chi}^0 \Gamma] v = v$, or with $v = [\tilde{\chi}^0]^{1/2} \tilde{v}$,

$$[\tilde{\chi}^0]^{1/2} \Gamma [\tilde{\chi}^0]^{1/2} \tilde{v} = \tilde{v}, \quad (12)$$

where the matrix is symmetric if Γ is symmetric. The relevant symmetric matrix reads,

$$M_{n_1, n_2} = \frac{1}{\beta} \sqrt{\tilde{\chi}^0(i\omega_{n_1})} [\Gamma^{(\text{pp})}(i\omega_{n_1}, i\omega_{n_2}; 0)] \sqrt{\tilde{\chi}^0(i\omega_{n_2})}, \quad (13)$$

and we have to find its largest eigenvalue. We have simplified the notation for the arguments for $\tilde{\chi}^0$ omitted the $\mathbf{q} = 0$ -label. In a DMFT calculation for a given temperature T , we first determine $\Sigma(i\omega_n)$ and the full particle-particle irreducible vertex $\Gamma^{(\text{pp})}(i\omega_{n_1}, i\omega_{n_2}; 0)$. The pair propagator $\tilde{\chi}^0(i\omega_{n_1})$ is obtained from Eq. (5). Then we can search for the largest eigenvalue of the symmetric matrix in Eq. (13) for the instability criterion.

B. Calculations in the superconducting phase

We also perform calculations in the superconducting phase. We work in Nambu space with matrices then. The local lattice Green's functions have the form

$$G_{11}(i\omega_n) = A_G \text{HT}[\rho_0](\varepsilon_+) + B_G \text{HT}[\rho_0](\varepsilon_-) \quad (14)$$

and

$$G_{21}(i\omega_n) = A_F \text{HT}[\rho_0](\varepsilon_+) + B_F \text{HT}[\rho_0](\varepsilon_-) \quad (15)$$

with $A_G = (\zeta_2(i\omega_n) + \varepsilon_+(i\omega_n))/(\varepsilon_+(i\omega_n) - \varepsilon_-(i\omega_n))$, $B_G = (\zeta_2(i\omega_n) + \varepsilon_-(i\omega_n))/(\varepsilon_-(i\omega_n) - \varepsilon_+(i\omega_n))$, $A_F = \Sigma_{21}(i\omega_n)/(\varepsilon_+(i\omega_n) - \varepsilon_-(i\omega_n))$, and $B_F = \Sigma_{21}(i\omega_n)/(\varepsilon_-(i\omega_n) - \varepsilon_+(i\omega_n))$, where

$$\varepsilon_{\pm} = \frac{\zeta_1(i\omega_n) - \zeta_2(i\omega_n)}{2} \pm \frac{1}{2} \sqrt{(\zeta_1(i\omega_n) + \zeta_2(i\omega_n))^2 - 4\Sigma_{21}(i\omega_n)\Sigma_{12}(i\omega_n)},$$

with $\zeta_1(z) = z + \mu - \Sigma_{11}(z)$ and $\zeta_2(z) = z - \mu - \Sigma_{22}(z)$. We have $G_{12}(i\omega_n) = G_{21}(i\omega_n)$ and $G_{22}(i\omega_n) = -G_{11}(-i\omega_n)$ for the Nambu Green's functions. We use $\Sigma_{12}(i\omega_n) = \Sigma_{21}(i\omega_n)$ and $\Sigma_{22}(i\omega_n) = -\Sigma_{11}(-i\omega_n)$ for the self-energies. This can be deduced from the properties of the corresponding Green's functions including the assumption of time-reversal symmetry. At half filling $G_{11}(i\omega_n)$ and $\Sigma_{11}(i\omega_n)$ are imaginary functions, whereas $G_{21}(i\omega_n)$ and $\Sigma_{21}(i\omega_n)$ and $D(i\omega_m)$ and $\Sigma_{\text{ph}}(i\omega_m)$ are real functions.

In the NRG approach we calculate the self-energy matrix for the effective impurity model from the matrix of higher Green's functions $\underline{F}(\omega)$ with $F_{11}(\omega) = \langle\langle c_{d,\uparrow} n_{\downarrow}; c_{d,\uparrow}^{\dagger} \rangle\rangle_{\omega}$, $F_{12}(\omega) = \langle\langle c_{d,\uparrow} n_{\downarrow}; c_{d,\downarrow} \rangle\rangle_{\omega}$, $F_{21}(\omega) = -\langle\langle c_{d,\downarrow} n_{\uparrow}; c_{d,\uparrow}^{\dagger} \rangle\rangle_{\omega}$ and $F_{22}(\omega) = -\langle\langle c_{d,\downarrow} n_{\uparrow}; c_{d,\downarrow} \rangle\rangle_{\omega}$. For the phonon part we use $M_{11}(\omega) = \langle\langle c_{d,\uparrow}(b + b^{\dagger}); c_{d,\uparrow}^{\dagger} \rangle\rangle_{\omega}$, $M_{12}(\omega) = \langle\langle c_{d,\uparrow}(b + b^{\dagger}); c_{d,\downarrow} \rangle\rangle_{\omega}$, $M_{21}(\omega) = -\langle\langle c_{d,\downarrow}^{\dagger}(b + b^{\dagger}); c_{d,\uparrow}^{\dagger} \rangle\rangle_{\omega}$ and $M_{22}(\omega) = -\langle\langle c_{d,\downarrow}^{\dagger}(b + b^{\dagger}); c_{d,\downarrow} \rangle\rangle_{\omega}$. In the NRG we calculate M_{11} and M_{21} directly on the real axis from the Lehman spectral representation. The others follow from $M_{12}(\omega) = -M_{21}(-\omega)^*$ and $M_{22}(\omega) = M_{11}(-\omega)^*$. We can define the self-energy matrix by

$$\underline{\Sigma}(\omega) = U \underline{F}(\omega) \underline{G}(\omega)^{-1} + g \underline{M}(\omega) \underline{G}(\omega)^{-1}. \quad (16)$$

For self-consistency the local lattice Green's functions $\underline{G}(\omega)$ has to be equal to the impurity Green's function, $\underline{\mathcal{G}}(\omega) = G(\omega)$, where

$$\mathcal{G}^{-1}(\omega) = \omega \mathbb{1}_2 + \mu \tau_3 - \underline{K}(\omega) - \underline{\Sigma}(\omega), \quad (17)$$

with the matrix $\underline{K}(\omega)$ describing the effective medium. We can take the form of the effective impurity model to correspond to an Anderson-Holstein impurity model⁴⁶ and calculations are carried out as detailed, for instance in Ref. 47. We solve the effective impurity problem with

the numerical renormalization group^{48,49} (NRG) adapted to the case with symmetry breaking. The NRG has been shown to be very successful for calculating the local dynamic response functions, and we use the approach^{50,51} based on complete basis set proposed by Anders and Schiller.⁵² For the logarithmic discretization parameter we take the value $\Lambda = 1.8$ and keep about 1000 states at each iteration. The initial bosonic Hilbert space is restricted to a maximum of 50 states. We will mainly consider two cases: (i) constant density of states $\rho_0 = 1/W$, where W is the bandwidth and (ii) the semi-elliptic DOS $\rho_0(\varepsilon) = \sqrt{4t^2 - \varepsilon^2}/(2\pi t^2)$ with $W = 4t = 2D$.

III. DIAGRAMMATIC CALCULATION FOR T_c

In this section we first show how the standard approach to conventional superconductivity, ME theory, would be applied to the model under consideration, and which diagrams are included. To determine T_c we use the instability criterion, Eq. (12), which is equivalent to the linearized ME equations.

A. Standard diagrammatics, ME theory

In ME theory the irreducible vertex in Eq. (13) is given by the full phonon propagator

$$\Gamma^{(\text{pp})}(i\omega_{n_1}, i\omega_{n_2}; i\omega_n = 0) = -g^2 D(i\omega_{n_1} - i\omega_{n_2}). \quad (18)$$

Diagrammatically this is depicted in Fig. 1 (a).

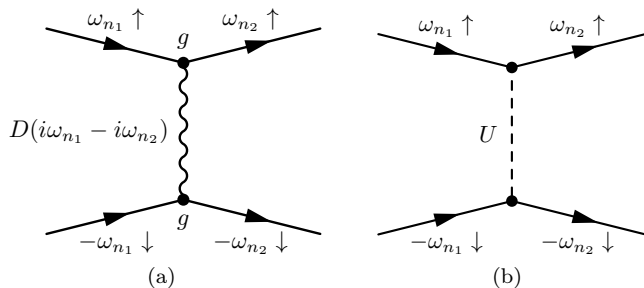


FIG. 1: Contributions to the irreducible vertex (a) electron-phonon part, (b) first order in U .

Due to Migdal's theorem¹¹ other vertex corrections including the phonon propagator are neglected. In general, the ME theory is a self-consistent calculation, and the electronic self-energy reads [see Fig. 2 (a)],

$$\Sigma(i\omega_n) = -\frac{g^2}{\beta} \sum_m G(i\omega_m + i\omega_n) D(i\omega_m). \quad (19)$$

The phonon self-energy reads [see Fig. 2 (b)],

$$\Sigma_{\text{ph}}(i\omega_m) = \frac{2g^2}{\beta} \sum_n G(i\omega_n) G(i\omega_m + i\omega_n). \quad (20)$$

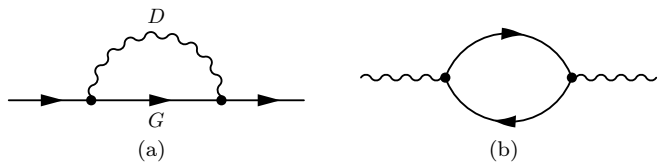


FIG. 2: Diagrams for (a) electronic self-energy and (b) the phonon self-energy.

We define ω_0^r as the relevant renormalized phonon scale, which is extracted from the peak position of the full phonon spectral function $\rho^D(\omega)$. The electronic Green's function $G(i\omega_n)$ is determined as in Eq. (6). An appropriate definition of the coupling constant λ is

$$\lambda = 2 \int_0^\infty d\omega \frac{\alpha^2 F(\omega)}{\omega}, \quad (21)$$

where we the pairing function is defined via a Fermi surface average,

$$\alpha^2 F(\omega) = \frac{1}{\rho_0^2} \sum_{\mathbf{k}, \mathbf{k}'} \alpha_{\mathbf{k}, \mathbf{k}'}^2 F(\omega) \delta(\varepsilon_{\mathbf{k}} - \mu) \delta(\varepsilon_{\mathbf{k}'} - \mu) \quad (22)$$

with

$$\alpha_{\mathbf{k}, \mathbf{k}'}^2 F(\omega) = \rho_0 |g_{\mathbf{k}, \mathbf{k}'}|^2 \rho_{\mathbf{k}-\mathbf{k}'}^D(\omega). \quad (23)$$

For the Holstein model using the free spectral function we have $\alpha^2 F(\omega) = \rho_0 g^2 [\delta(\omega - \omega_0) - \delta(\omega + \omega_0)]$, such that we obtain $\lambda_0 = \rho_0 2g^2/\omega_0$, purely in terms of bare parameters. However, more relevant is the effective coupling λ for the Holstein model is given by the full renormalized phonon propagator,¹³

$$\lambda = 2\rho_0 g^2 \int_0^\infty d\omega \frac{\rho^D(\omega)}{\omega} = -\rho_0 g^2 D(0). \quad (24)$$

The dimensionless quantity for the Coulomb interaction corresponding to λ_0 is $\mu_c = \rho_0 U$.

In a self-consistent numerical calculation for a given temperature T , we first determine $\Sigma(i\omega_n)$ and $\Sigma_{\text{ph}}(i\omega_m)$ by iterating Eqs. (19) and (20) and thus $G(i\omega_n)$ and $D(i\omega_m)$. Then we determine $\tilde{\chi}^0(i\omega_{n_1})$ from Eq. (5). $D(i\omega_m)$ is used in Eq. (18) to determine the irreducible vertex. Then we calculate the largest eigenvalue of the symmetric matrix in Eq. (13) for the instability criterion. Instead of calculating the phonon Green's function self-consistently we can also take it as an input. Using the DMFT results for $D(i\omega_m)$ we found in previous work¹³ that T_c obtained from this procedure agrees well with the full DMFT result as long as the renormalized Migdal condition, $\lambda\omega_0^r/W$ small, is satisfied. In the DMFT calculation $\Gamma^{(\text{pp})}$ and $\Sigma(i\omega_n)$ contain all higher order corrections.

In the usual theory the Coulomb repulsion is included directly up to first order or as an additional empirical

parameter μ^* . The vertex has then two contributions, one as before due to the electron-phonon interaction, and the second one from the Coulomb repulsion [see Fig. 1 (b)],

$$\Gamma^{(\text{pp})}(i\omega_{n_1}, i\omega_{n_2}; i\omega_n = 0) = -g^2 D(i\omega_{n_1} - i\omega_{n_2}) - U. \quad (25)$$

The eigenvalue equation (12) with the pairing vertex (25) can be solved analytically with approximations similar to the ones by McMillan.⁵³ This yields

$$T_c = \frac{2C\omega_0^r}{\pi} \exp\left[-\frac{Z}{\lambda - \mu_c^*[1 + \frac{1}{2}\lambda]}\right], \quad (26)$$

with $C = e^\gamma \approx 1.78$ with the Euler-Mascheroni constant $\gamma = 0.57721$. We have introduced $Z = 1 - \lim_{\omega \rightarrow 0} \Sigma(i\omega)/i\omega$ and μ_c^* is given by Eq. (1) with $E_{\text{el}} = D$ and $\omega_{\text{ph}} = \omega_0^r$. This corresponds to the result by McMillan⁵³ or Allen and Dynes⁵⁴,

$$T_c = \frac{\langle \omega \rangle}{1.2} e^{-\frac{1.04(1+\lambda)}{\lambda - \mu_c^*(1+0.62\lambda)}}, \quad (27)$$

where $Z = 1 + \lambda$ is used. The essential feature is that the Coulomb repulsion, which is the same for all $i\omega_n$ is effectively reduced from μ_c to μ_c^* when counteracting the electron-phonon attraction with strength λ . This shows how retardation effects assist the electron-phonon induced superconductivity by suppressing the detrimental effects due to the Coulomb repulsion.

In summary, the diagrams in Figs. 1 and 2 are the ones included in the standard theory of superconductivity. Usually, the phonons are not calculated self-consistently but rather taken as an input, for instance from DFT calculations or from experiment. Also μ_c^* is usually not calculated but used as a fitting parameters. In the following we consider higher order corrections to the standard approach.

B. Higher order terms

The perturbation expansion for two different interactions is rather involved, since terms of each perturbation series as well as mixtures can appear. In a skeleton expansion higher order contributions can be grouped into the following terms for self-energies and vertex functions:

1. Contributions to the full electron-phonon vertex $\Gamma^{(\text{ep})} = \Gamma_g^{(\text{ep})} + \Gamma_U^{(\text{ep})} + \Gamma_{g,U}^{(\text{ep})}$, where the bare vertex is $\Gamma_0^{(\text{ep})} = g$:
 - (a) Higher order corrections $\Gamma_g^{(\text{ep})}$ purely due to g , not including $\Gamma_0^{(\text{ep})}$.

- (b) Contributions $\Gamma_U^{(\text{ep})}$ which include the bare vertex $\Gamma_0^{(\text{ep})}$ and higher order terms purely due to U .
- (c) Higher order corrections $\Gamma_{g,U}^{(\text{ep})}$ due to mixed terms of g and U , not including $\Gamma_0^{(\text{ep})}$.

2. Contributions to the phonon self-energy Σ_{ph} :

- (a) Higher order contributions to Σ_{ph} , which can be written in terms of $\Gamma_g^{(\text{ep})}$, i.e., purely due to g .
- (b) Contributions to Σ_{ph} due to mixed terms of g and U . These can be expressed in terms of $\Gamma_U^{(\text{ep})}$ or $\Gamma_{g,U}^{(\text{ep})}$.

3. Contributions to the electron self-energy Σ :

- (a) Contributions to Σ , which can be written in terms of $\Gamma_g^{(\text{ep})}$, i.e. purely due to g .
- (b) Contributions to Σ purely due to U .
- (c) Contributions to Σ due to mixed terms, which can be expressed in terms of $\Gamma_U^{(\text{ep})}$ or $\Gamma_{g,U}^{(\text{ep})}$.
- (d) Contributions to Σ due to mixed terms, which can not be written in terms of $\Gamma^{(\text{ep})}$.

4. Contributions to the irreducible vertex $\Gamma^{(\text{pp})}$:

- (a) Contributions to $\Gamma^{(\text{pp})}$ purely due to U .
- (b) Contributions to $\Gamma^{(\text{pp})}$ due to g and U , which can be written in terms of full propagators and the electron-phonon vertex $\Gamma^{(\text{ep})}$.
- (c) Contributions to $\Gamma^{(\text{pp})}$ due to g and U , which can not be written in terms of $\Gamma^{(\text{ep})}$.

We assume in the following that the parameters are chosen such that higher order contributions of the type $\Gamma_g^{(\text{ep})}$, i.e., 1(a), 2(a) and 3(a), are small due to Migdal's theorem. By taking the full phonon propagator from the DMFT calculation as in previous work,¹³ we avoid considering in detail effects of 2(b), and rather assume that we can include the correct phonon propagator. We focus on contributions 1(b), 3(b,c), and 4(a)(b), in the following, which are the main contributions in the low order perturbation theory. Contributions to the type 1(c), 3(d) and 4(c) include higher order diagrams and will not be considered explicitly here.

We can generally write contributions to the pairing vertex of the form 4(b) as

$$\Gamma^{(\text{pp})}(i\omega_{n_1}, i\omega_{n_2}; i\omega_n = 0) = -\Gamma_U^{(\text{ep})}(i\omega_{n_1}, i\omega_{n_2})D(i\omega_{n_1} - i\omega_{n_2})\Gamma_U^{(\text{ep})}(-i\omega_{n_1}, -i\omega_{n_2}), \quad (28)$$

where $\Gamma_U^{(\text{ep})}$ includes g and all corrections due to U , see Fig. 3.

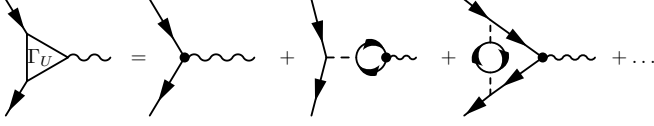


FIG. 3: Contributions to the electron-phonon vertex $\Gamma_U^{(\text{ep})}$.

For $\Gamma_U^{(\text{ep})}(i\omega_{n_1}, i\omega_{n_2})$, $i\omega_{n_1}$ is the ingoing electronic frequency, $i\omega_{n_2}$ the outgoing one and the bosonic one is $i\omega_{n_1} - i\omega_{n_2}$. $D(i\omega_n)$ is the full propagator including corrections due to U and g . Diagrammatically, these contributions to $\Gamma^{(\text{pp})}$ are displayed in Fig. 4 (a).

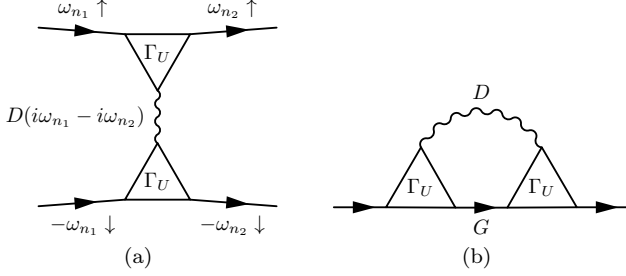


FIG. 4: (a) Higher order terms involving vertex corrections of the electron-phonon vertex. (b) Electronic self-energy including vertex corrections for the electron-phonon vertex.

The higher order corrections included in Eq. (28) can be seen as a redefinition of λ defined in (24). The vertex $\Gamma_U^{(\text{ep})}$ does not vary much up to the small phonon scale, such that we can write approximately with $g^r = \Gamma_U^{(\text{ep})}(0, 0)$,

$$\lambda \simeq 2\rho_0 [g^r]^2 \int_0^\infty d\omega \frac{\rho^D(\omega)}{\omega} = -\rho_0 [g^r]^2 D(0), \quad (29)$$

where $\rho^D(\omega)$ can also include self-energy corrections due to U . Such a redefined λ enters the approximate results for T_c such as Eq. (26). We can also take into account the effect that $\Gamma_U^{(\text{ep})}$ is a function of frequency and average over a range given by the phonon Green's function such that

$$[g^r]^2 = \frac{1}{N_D} \sum_{n_2} \Gamma_U^{(\text{ep})}(0, i\omega_{n_2})^2 D(i\omega_{n_2}), \quad (30)$$

where $N_D = \sum_{n_2} D(i\omega_{n_2})$.

We now consider the diagrams contributing to the electron-phonon vertex $\Gamma_U^{(\text{ep})}$. Some of them are shown in Fig. 3. To order Ug we have

$$\Gamma_U^{(\text{ep},1)}(i\omega_{n_1}, i\omega_{n_2}) = g[1 + U\Pi(i\omega_{n_1} - i\omega_{n_2})], \quad (31)$$

where the particle-hole bubble is given by

$$\Pi(i\omega_n) = \frac{1}{\beta} \sum_m G(i\omega_n + i\omega_m) G(i\omega_m). \quad (32)$$

$\Pi(0)$ can be evaluated analytically at $T = 0$ and one finds for the constant density of states $\Pi(0) = -2 \log(2)\rho_0$ and for the semi-elliptic DOS $\Pi(0) = -\frac{4}{3}\rho_0$. It turns out that a good empirical form for $\Pi(i\omega)$ is given by

$$\Pi(i\omega) = \frac{-a\rho_0}{1 + b_1|\omega| + b_2\omega^2}. \quad (33)$$

If $G(i\omega_n)$ is the non-interacting Green's function in Eq. (32) then $a = 4/3$ for the semi-elliptic DOS. In this case we find that $b_1 = 1.3/D$ and $b_2 = 1.63/D^2$ give a good fit.

We can sum up a whole series of diagrams of the type discussed in Eq. (31) which corresponds to screening on the RPA level,

$$\Gamma_U^{(\text{ep,RPA})}(i\omega_{n_1}, i\omega_{n_2}) = \frac{g}{1 - U\Pi(i\omega_{n_1} - i\omega_{n_2})}. \quad (34)$$

Note the absence of a factor 2 in the denominator for the Hubbard interaction. Since $\Pi < 0$ these diagrams lead to an effective reduction of the electron-phonon coupling. If one assumes that Π does not change much on the phonon scale enforced via $D(i\omega_m)$, then one could approximate $g^r = g/[1 - U\Pi(0)]$, and for the Bethe lattice $g^r = g/[1 + 4\mu_c/3]$.

There are three diagrams to order U^2 in addition to the screening term to correct the vertex (see the third diagram in the Fig. 3 and Fig. 5).

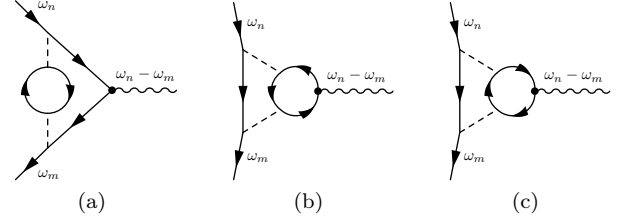


FIG. 5: Vertex corrections to the electron-phonon vertex to order gU^2 .

The first term, Fig. 5 (a), reads,

$$\Gamma_U^{(\text{ep},2,1)}(i\omega_n, i\omega_m) = -\frac{gU^2}{\beta} \sum_k \Pi(i\omega_k) G(i\omega_k + i\omega_n) \times G(i\omega_k + i\omega_m). \quad (35)$$

The second one, Fig. 5 (b), is of the form

$$\Gamma_U^{(\text{ep},2,2)}(i\omega_n, i\omega_m) = -\frac{gU^2}{\beta} \sum_k \Pi_{pp}(i\omega_k) G(i\omega_k - i\omega_n) \times G(i\omega_k - i\omega_m), \quad (36)$$

where we have introduced the particle-particle bubble,

$$\Pi_{pp}(i\omega_n) = \frac{1}{\beta} \sum_m G(i\omega_n - i\omega_m) G(i\omega_m). \quad (37)$$

At half filling we have $G(-i\omega_m) = -G(i\omega_m)$, which implies $\Pi_{pp}(i\omega_n) = -\Pi(i\omega_n)$. With this one obtains

$$\Gamma_U^{(\text{ep},2,2)}(i\omega_n, i\omega_m) = -\Gamma_U^{(\text{ep},2,1)}(i\omega_n, i\omega_m), \quad (38)$$

and the first diagram is canceled. The third diagram, Fig. 5 (c), is like the first one $\Gamma_U^{(\text{ep},2,3)}(i\omega_n, i\omega_m) = \Gamma_U^{(\text{ep},2,1)}(i\omega_n, i\omega_m)$. So altogether we have just one contribution of the form (35) at half filling. Diagrams of these type together with the RPA screening series were discussed by Huang et al.⁵⁵ for the two dimensional Hubbard-Holstein model. The full electron-phonon vertex was calculated with QMC. It was found that for values of U up to half the bandwidth the diagrammatics and the non-perturbative result are in good agreement. However, for large values of U , the perturbation theory breaks down.

As can be seen from this analysis of the vertex correction, there is a considerable effect to suppress the coupling g when U is finite. Including diagrams in Eq. (34) and (35) we can write the approximate form,

$$\frac{g^r}{g} = \frac{1}{1 + a\mu_c} - b\mu_c^2, \quad (39)$$

where $a = -\Pi(0)/\rho_0$ and

$$b = \frac{1}{\rho_0^2\beta} \sum_k \Pi(i\omega_k)G(i\omega_k)^2. \quad (40)$$

In the simplest case for free Green's functions and a semi-elliptic DOS we have $a = 4/3$ and $b = 0.8237$ numerically. In a calculation strictly up to second order in U we have instead of Eq. (39),

$$\frac{g^r}{g} = 1 - a\mu_c + (a^2 - b)\mu_c^2, \quad (41)$$

We plot results for $(g^r/g)^2$ in Fig. 6.

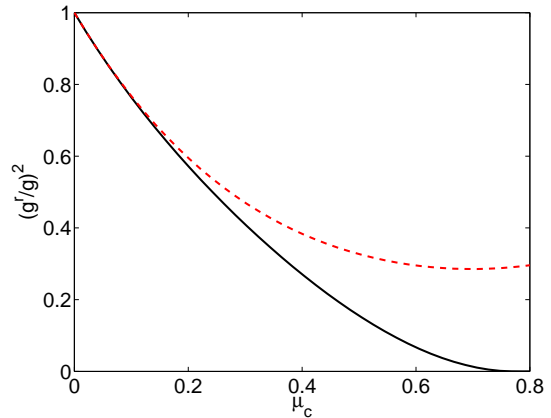


FIG. 6: (Color online) $(g^r/g)^2$ as a function of μ_c , full line according to Eq. (39) and dashed line according to Eq. (41).

We see that there occurs a substantial suppression, such that already for $\mu_c = 0.25$ the quantity $(g^r/g)^2$ is reduced to about a half of its value for $\mu_c = 0$. Since $a^2 > b$, the second term in Eq. (41) which dominates for larger μ_c , leads to an upturn of the result. The result in Eq. (39) overestimate the suppression effect for large values of μ_c .⁵⁵ For the interacting system, the coefficients a and b tend to be smaller than the values in the non-interacting limit.

The vertex corrections $\Gamma_U^{(\text{ep})}$ also enter the electronic self-energy as one class of diagrams contributing to 3(c). This can be written as

$$\Sigma(i\omega_n) = -\frac{1}{\beta} \sum_m \Gamma_U^{(\text{ep})}(i\omega_n, i\omega_m + i\omega_n)G(i\omega_m + i\omega_n)D(i\omega_m)\Gamma_U^{(\text{ep})}(i\omega_m + i\omega_n, i\omega_n). \quad (42)$$

This is shown diagrammatically in Fig. 4 (b). As discussed above, there are also other types of mixed diagrams 3(d), which cannot be written in the form of Eq. (42).

C. Higher order corrections from purely U

We now deal with the higher order corrections purely from U , i.e., of type 4(a). We will restrict our attention only to the terms second order in U . The corresponding contribution (crossed diagram) to the pairing vertex

reads

$$\Gamma^{(\text{pp})}(i\omega_{n_1}, i\omega_{n_2}; i\omega_n = 0) = U^2\Pi(i\omega_{n_1} + i\omega_{n_2}). \quad (43)$$

The diagram is depicted in Fig. 7 (a).

A naive way of taking this into consideration would be to assume that $\Pi(i\omega_{n_1} + i\omega_{n_2})$ varies little for the scales under considerations, such that for all frequencies we can assume $-\rho_0 U^2 \Pi(0) = a\mu_c^2$. Then this term can be treated in the same way as the first order term in U , where we can simply write $\mu_c \rightarrow \bar{\mu}_c = \mu_c + a\mu_c^2$. This quantity is then subject to the full retardation effects and becomes

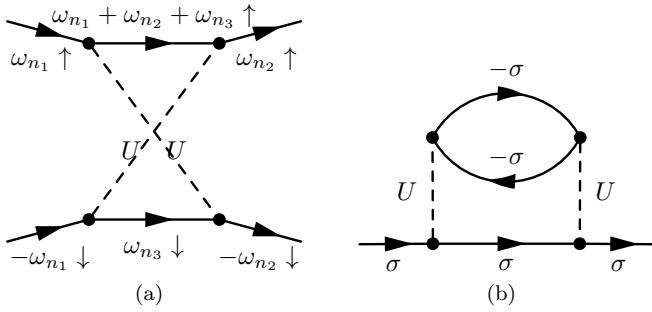


FIG. 7: (a) Higher order diagram vertex contribution from the Coulomb repulsion. (b) Second order in U diagram for electronic self-energy.

$\bar{\mu}_c^*$,

$$\bar{\mu}_c^* = \frac{\bar{\mu}_c}{1 + \bar{\mu}_c \log(\frac{D}{\omega_{\text{ph}}})}, \quad (44)$$

However, as analyzed in detail in Sec. V retardation effects are less efficient for the second order term when the decay of $\Pi(i\omega)$ is taken into account properly.

For the self-energy contributions of type 3(b), we will only consider the standard second order diagram depicted in Fig. 7 (b),

$$\Sigma(i\omega_n) = -\frac{U^2}{\beta^2} \sum_{n_1, n_2} G(i\omega_n - i\omega_{n_1}) G(i\omega_{n_1} + i\omega_{n_2}) G(i\omega_{n_2}). \quad (45)$$

IV. DIAGRAMMATIC CALCULATION FOR THE SUPERCONDUCTING STATE

In this section we consider calculations in the superconducting state. We first present the application of the standard theory to the HH model and then discuss higher order corrections. These calculations allow us, for instance, to study the gap at $T = 0$. The relevant quantities are matrices in Nambu space. We have to calculate the diagonal and off-diagonal components of the self-energy. First we present the diagrams usually used in the standard ME approach.

A. Standard diagrammatics, ME theory

To lowest order the diagonal self-energy is given by

$$\Sigma_{11}(i\omega_n) = -\frac{g^2}{\beta} \sum_m G_{11}(i\omega_m + i\omega_n) D(i\omega_m), \quad (46)$$

and the off-diagonal self-energy reads,

$$\Sigma_{21}(i\omega_n) = \frac{g^2}{\beta} \sum_m G_{21}(i\omega_m + i\omega_n) D(i\omega_m). \quad (47)$$

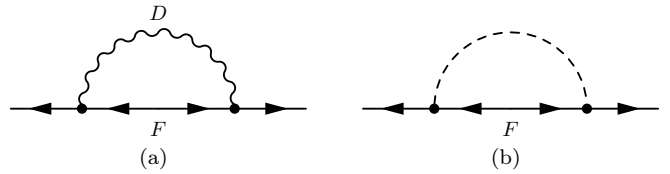


FIG. 8: Diagrams for the off-diagonal self-energy (a) from electron-phonon interaction and (b) for the Coulomb repulsion with the notation $F = G_{21}$.

This is depicted in Fig. 8 (a) with the off-diagonal self-energy marked as F .

In the limit of low temperature, $T \rightarrow 0$, we use

$$\frac{1}{\beta} \sum_n f(i\omega_n) \rightarrow \frac{1}{2\pi} \int_{-\infty}^{\infty} d\omega f(i\omega). \quad (48)$$

For the off-diagonal self-energy [see Fig. 8 (b)] we have the Coulomb contribution ($\eta \rightarrow 0$)

$$\Sigma_{21}(i\omega_n) = \frac{U}{\beta} \sum_m G_{21}(i\omega_m) e^{i\omega_m \eta}. \quad (49)$$

Since $G_{21}(i\omega_m)$ decays sufficiently rapidly the factor $e^{i\omega_m \eta}$ is usually not needed.

These are the equations, which are taken into account in the standard theory. Often, the Coulomb term is then projected onto the phonon scale (Coulomb pseudopotential), where only the reduced value μ_c^* enters. Making a few simplifying assumption (see Sec. VB) we can derive for the spectral gap at $T = 0$, $\Delta_{\text{sp}} \simeq \Sigma_{21}(0)/Z$,

$$\Delta_{\text{sp}} = 2\omega_0^T e^{-\frac{Z}{\lambda - \mu_c^*(1 + \frac{\lambda}{2})}}. \quad (50)$$

This result is very similar to the one for T_c . Equations (46), (47), and (49) correspond to the standard approach for the theory of conventional superconductivity.^{7,8}

B. Higher order corrections

In a similar way as for the analysis of the pairing vertex in Sec. III, we can classify terms for the self-energy into different contributions. We will follow the same logic as in the calculation for T_c and focus on the same type of diagrams as before. Here we consider a subclass of type 3(c), which includes Coulomb vertex corrections of the electron-phonon vertex of the type $\Gamma_U^{(\text{ep})}$. It reads,

$$\Sigma_{11}(i\omega_n) = -\frac{1}{\beta} \sum_m \Gamma_U^{(\text{ep})}(i\omega_n, i\omega_m + i\omega_n) G_{11}(i\omega_m + i\omega_n) D(i\omega_m) \Gamma_U^{(\text{ep})}(i\omega_m + i\omega_n, i\omega_n). \quad (51)$$

Assuming a slow variation of Γ_U on the phonon, scale a good approximation is of the form,

$$\Sigma_{11}(i\omega_n) \simeq -\frac{[g^r]^2}{\beta} \sum_{m_1} D(i\omega_{m_1}) G_{11}(i\omega_n + i\omega_{m_1}). \quad (52)$$

Similarly we have for the off-diagonal self-energy,

$$\Sigma_{21}(i\omega_n) = \frac{1}{\beta} \sum_m \Gamma_U^{(\text{ep})}(i\omega_n, i\omega_m + i\omega_n) G_{21}(i\omega_m + i\omega_n) D(i\omega_m) \Gamma_U^{(\text{ep})}(i\omega_m + i\omega_n, i\omega_n). \quad (53)$$

For $\Gamma_U^{(\text{ep})}(i\omega_n, i\omega_m)$ we consider the same diagrams as in Sec. III B. We assume that $D(i\omega_m)$ is the full phonon

propagator and hence it contains corrections due to U as well.

C. Higher order corrections from purely U

Of the contributions of the type 3(b) we discuss all terms to second order in U . In the Nambu perturbation theory ones has (cf. Ref. 56),

$$\Sigma_{11,U}^{(2,1)}(i\omega_n) = -\left(\frac{U}{\beta}\right)^2 \sum_{m_1, m_2} G_{11}(i\omega_n + i\omega_{m_1}) G_{22}(i\omega_{m_2}) G_{22}(i\omega_{m_1} + i\omega_{m_2}). \quad (54)$$

and

$$\Sigma_{11,U}^{(2,2)}(i\omega_n) = \left(\frac{U}{\beta}\right)^2 \sum_{m_1, m_2} G_{21}(i\omega_n + i\omega_{m_1}) G_{12}(i\omega_{m_2}) G_{22}(i\omega_{m_1} + i\omega_{m_2}). \quad (55)$$

For the off-diagonal part we have

$$\Sigma_{21,U}^{(2,1)}(i\omega_n) = -\left(\frac{U}{\beta}\right)^2 \sum_{m_1, m_2} G_{21}(i\omega_n + i\omega_{m_1}) G_{12}(i\omega_{m_2}) G_{12}(i\omega_{m_1} + i\omega_{m_2}), \quad (56)$$

$$\Sigma_{21,U}^{(2,2)}(i\omega_n) = \left(\frac{U}{\beta}\right)^2 \sum_{m_1, m_2} G_{11}(i\omega_n + i\omega_{m_1}) G_{22}(i\omega_{m_2}) G_{12}(i\omega_{m_1} + i\omega_{m_2}). \quad (57)$$

The first diagram $\Sigma_{11,U}^{(2,1)}(i\omega_n)$ is the well known U^2 -diagram which gives the first dynamic correction, also in the normal phase as in Eq. (45). In comparison $\Sigma_{11,U}^{(2,2)}(i\omega_n)$ gives a smaller contribution as it is proportional to two off-diagonal Green's function. $\Sigma_{21,U}^{(2,1)}(i\omega_n)$ is also comparably small, but $\Sigma_{21,U}^{(2,2)}(i\omega_n)$ gives a sizeable reduction of the superconducting state. We can see this by writing it as

$$\Sigma_{21,U}^{(2,2)}(i\omega_n) = -U^2 \frac{1}{\beta} \sum_{m_1} \Pi(i\omega_n + i\omega_{m_1}) G_{21}(i\omega_{m_1}). \quad (58)$$

where $\Pi(i\omega_n)$ is given in Eq. (32) with $G(i\omega_m) = G_{11}(i\omega_m)$.

For small $i\omega_n$ a crude approximation is to write

$$\Sigma_{21,U}^{(2,2)}(0) \simeq -U^2 c_1 \Pi(0) \frac{1}{\beta} \sum_{m_1} G_{21}(i\omega_{m_1}), \quad (59)$$

where it is assumed that $G_{21}(i\omega_{m_1})$ is only finite in small interval such that we can take $\Pi(i\omega_n)$ constant. Hence we find a direct correction to the term $\Sigma_{21,U}^{(1)}$. With the

result for $\Pi(0)$, one has then approximately

$$\Sigma_{21,U}^{(1)} + \Sigma_{21,U}^{(2,2)}(0) \simeq U(1 + a\mu_c) \frac{1}{\beta} \sum_{m_1} G_{21}(i\omega_{m_1}), \quad (60)$$

This is the same effect that was discussed for T_c and the crossed diagram [see Fig. 7 (a)] where naively the effective μ_c becomes $\bar{\mu}_c = \mu_c(1 + a\mu_c)$. In a more accurate treatment, we have to take the frequency dependence into account, and we will see that this leads to modifications.

V. ANALYTIC AND NUMERICAL RESULTS FOR μ_c^*

In the last two sections we have analyzed the diagrammatic expansion for the model in Eq. (2) and discussed certain types of diagrams. In this section we want to specifically study the pseudopotential effect without including all other corrections. We are interested whether the first and second order calculations give qualitatively different results for μ_c^* . We present a combination of analytical and numerical arguments. In the literature, there exist a number of ways to calculate μ_c^* for a given microscopic model. One early approach by Bogoliubov et al. is based on an integral equation for the Coulomb part in the pairing equation.^{9,18} Morel and Anderson¹⁷ gave an approximate solution for the Migdal-Eliashberg equations including a screened Coulomb repulsion in the $T = 0$ formalism. The pseudopotential μ_c^* also appears naturally when superconducting pairing instabilities are studied in a renormalization group framework.^{44,57} In the following we first calculate μ_c^* directly by projecting the pairing matrix to low energy. Analytic and numerical results are compared. Then in a second approach we calculate Δ_{sp} from an approximate solution of the self-consistency equation and thus extract μ_c^* . Finally we also compute numerical results for T_c obtained from the instability condition and analyze these results in terms of μ_c^* .

A. Projection scheme

The starting point for the projection approach is the pairing matrix in the form

$$A_{nm} = \delta_{nm} - M_{nm}, \quad (61)$$

where M_{nm} is given in Eq. (13). This matrix becomes singular at T_c . We introduce the “low-energy part”

$$A_{nm}^{\text{low}} = A_{nm} - \sum_{|\omega'_n|, |\omega'_m| > \omega_{\text{ph}}} A_{nn'} [\bar{A}^{-1}]_{n'm'} A_{m'm}, \quad (62)$$

n, m such that $|\omega_n|, |\omega_m| < \omega_{\text{ph}}$, and \bar{A} is the matrix that is left after the blocks given by $|\omega_n| < \omega_{\text{ph}}$ or $|\omega_m| < \omega_{\text{ph}}$ were removed. If \bar{A}^{-1} is not singular, Eq. (61) and Eq. (62) become singular for the same parameters. This

way we can reduce the matrix size so that it only includes frequencies for which the electron-phonon interaction is important. The “folding in” of larger frequencies then describes how retardation effects reduce the effects of the Coulomb repulsion on low frequency properties.

We first consider the lowest order term of $\Gamma^{(\text{pp})}$ in U namely $\Gamma^{(\text{pp})} = -U$. We want to focus on the dependence on the half-band width D and assume that the density of states scales as

$$\rho(\varepsilon) = \frac{1}{2D} \bar{\rho}\left(\frac{\varepsilon}{2D}\right), \quad (63)$$

where $\bar{\rho}$ is independent of D . For simplicity we assume in the following that $\bar{\rho}(x) = 1$ is a constant for $|x| \leq 1/2$ and zero otherwise, such that $\rho_0 = 1/(2D)$. It is then a rather good approximation to write

$$\tilde{\chi}^0(i\omega_n) = \begin{cases} \rho_0 \pi / |\omega_n|, & \text{if } |\omega_n| < D; \\ 0, & \text{otherwise.} \end{cases} \quad (64)$$

The matrix A then takes the form

$$A_{nm} = \delta_{nm} + \frac{\pi}{\beta \sqrt{|\omega_n \omega_m|}} \mu_c, \quad (65)$$

which is separable and can be inverted exactly. We obtain

$$[\bar{A}^{-1}]_{nm} = \delta_{nm} - \frac{\pi \mu_c}{\beta \sqrt{|\omega_n \omega_m|} [1 + \pi \mu_c / \beta \sum'_k 1/|\omega_k|]}, \quad (66)$$

where \sum'_k involves a summation over $|\omega_k| > \omega_{\text{ph}}$. Replacing the summations in Eqs. (62, 66) by integrals, we find

$$\begin{aligned} A_{nm}^{\text{low}} &= \delta_{nm} + \frac{\pi}{\beta \sqrt{|\omega_n \omega_m|}} \mu_c \\ &\quad - \frac{\pi}{\beta \sqrt{|\omega_n \omega_m|}} \frac{\mu_c^2 \log(D/\omega_{\text{ph}})}{1 + \mu_c \log(D/\omega_{\text{ph}})} \\ &= \delta_{nm} + \frac{\pi}{\beta \sqrt{|\omega_n \omega_m|}} \frac{\mu_c}{1 + \mu_c \log(D/\omega_{\text{ph}})}. \end{aligned} \quad (67)$$

Comparison of Eq. (65) and (67) leads to the Coulomb pseudopotential, $\mu_c \rightarrow \mu_c^*$, as given in in Eq. (1), and it is the result of Morel and Anderson.¹⁷

We next consider the second order term of $\Gamma^{(\text{pp})}$ in U [Eq. (43)]. Because of the form of $\Pi(i\omega_n + i\omega_m)$ it is then not possible to invert \bar{A} in Eq. (62) analytically. For the density of states [Eq. (63)] we can rewrite $\Pi(i\omega_n + i\omega_m)$ as

$$\Pi(i\omega_n + i\omega_m) = -\frac{1}{2D} f\left(\frac{\omega_n + \omega_m}{2D}\right), \quad (68)$$

where f is independent of D . As in Eq. (33) it is quite accurate to approximate f as

$$f(x) = \frac{a}{1 + b|x| + cx^2}, \quad (69)$$

where $a = 1.38$, $b = 2$ and $c = 5$ are suitable values for the constant DOS.

We now want to calculate A^{low} in Eq. (62) to third order in U . We use the result for \bar{A}^{-1} in Eq. (66), which neglects the second order term and is therefore only correct to order U . However, since the off-diagonal terms of A in Eq. (62) are of the order U , the final result is of the order U^3 . We obtain

$$\begin{aligned} & \sum_{nm} A_{1n} [\bar{A}^{-1}]_{nm} A_{m1} \\ &= \tilde{\chi}^0(i\omega_1) \left(\frac{U}{\beta}\right)^2 \sum_{|\omega_n| \geq \omega_{\text{ph}}} \tilde{\chi}^0(i\omega_n) \left[1 + \mu_c f\left(\frac{\omega_n}{2D}\right)\right]^2 \\ & - \left(\frac{U}{\beta}\right)^3 \frac{\tilde{\chi}^0(i\omega_1)}{1 + \mu_c \log(D/\omega_{\text{ph}})} \\ & \times \left\{ \sum_{|\omega_n| \geq \omega_{\text{ph}}} \tilde{\chi}^0(i\omega_n) \left[1 + \mu_c f\left(\frac{\omega_n}{2D}\right)\right] \right\}^2, \end{aligned} \quad (70)$$

where we focus on the diagonal result for the lowest frequency ω_1 . Using the definition of $\tilde{\chi}^0(i\omega_n)$ in Eq. (5), not the approximation in Eq. (64), and applying the limit $\omega_{\text{ph}} \ll D$, we calculate the sums

$$\sum_{|\omega_n| \geq \omega_{\text{ph}}} \tilde{\chi}^0(i\omega_n) f\left(\frac{\omega_n}{2D}\right)^k = \frac{a^k \beta}{2D} \log\left(\frac{DA_k}{\omega_{\text{ph}}}\right), \quad (71)$$

where $A_0 \approx 1.00$, $A_1 \approx 0.32$ and $A_2 \approx 0.20$. For $k = 1$ and 2 the denominator of f reduces the integral for large $|\omega_n|$, which effectively reduces the band width by a factor A_k . This reduction is naturally larger for $k = 2$ than for $k = 1$.

We now make an ansatz for μ_c^*

$$\mu_c^* = \frac{\mu_c + a\mu_c^2}{1 + \mu_c \log\left(\frac{D}{\omega_{\text{ph}}}\right) + a\mu_c^2 \log\left(\frac{D}{\omega_{\text{ph}}} A_{22}\right)}, \quad (72)$$

along the lines of the Morel-Anderson form, but including a second order term and a corresponding logarithm. Based on Eq. (71) we expect the effective band width to be smaller for the second order term and we therefore allow for a different multiplying factor A_{22} in the logarithm. Since the result in Eq. (70) is correct to order U^3 the factor A_{22} in Eq. (72) can be identified, $A_{22} = A_1^2/A_0 \approx 0.10$. The ansatz in Eq. (72) is then also correct to order U^3 .

Fig. 9 shows the results obtained by performing the calculations in Eq. (62) numerically using the first or second order result in U for $\Gamma^{(\text{pp})}$, and without introducing the approximation in Eq. (64). The figure also shows the analytical result in Eq. (72). The second order result is clearly larger than the first order result. For $\mu_c \lesssim 0.5$, Eq. (72) describes the full second order calculation rather well, while for larger μ_c there are corrections to the analytic result which make μ_c^* still larger compared to Eq. (72).

It is interesting to discuss the origin of the factor A_{22} in Eq. (72). In the present language the term $\log(D/\omega_{\text{ph}})$ in the first order calculation arises from ‘‘folding in’’ large

frequency contributions from U in Eq. (62), which extend to approximately $\omega \sim D$. The second order term in U is ‘‘folded in’’ in a similar way. However, as shown by Eq. (69), the contribution from large frequencies is reduced, leading to the effective band width being reduced by some factor for the second order contribution. This reduction factor is surprisingly large (1/10). The origin can be seen in Eq. (70), where the relevant terms are a product of the first and second order contributions in the first term, containing a factor two, and the first order contribution in the second term. The prefactor two of the logarithm in the first contribution leads to the factor A_1^2 , and thereby a very small factor.

This shows that the second order terms contribute to retardation effects, like the first order contribution. However, the reduction is substantially less efficient, as described by the small factor A_{22} . The band width therefore has to be very large to make this contribution to retardation efficient.

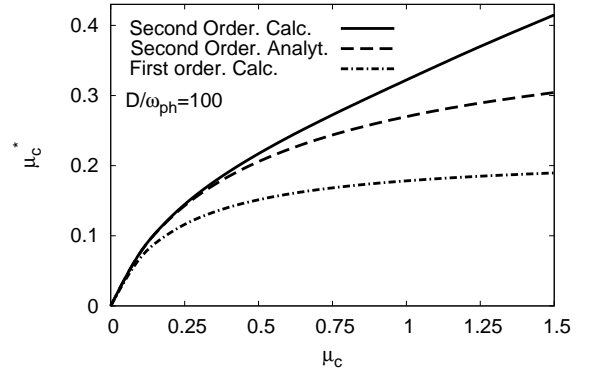


FIG. 9: The pseudopotential μ_c^* as a function of μ_c for $D/\omega_{\text{ph}} = 100$ and $\beta\omega_{\text{ph}} = 240$. The figure shows the calculated results using both the first order and first plus second order result for $\Gamma^{(\text{pp})}$ as well as the approximation in Eq. (72).

It is interesting to consider the second order contribution alone. We can then calculate results accurate up to order U^4 . The matrix \bar{A}^{-1} can be approximated by a unit matrix. Making an ansatz for μ_c^* and identifying with the fourth order result, we obtain

$$\mu_c^* = \frac{a\mu_c^2}{1 + a\mu_c^2 \log\left(\frac{DA_2}{\omega_{\text{ph}}}\right)}, \quad (73)$$

where $A_2 = 0.20$ was given above. The result of a full calculation is compared with the analytical approximation [Eq. (73)] in Fig. 10. Also in this case the analytical result agrees rather well with the full calculation for $\mu_c \lesssim 0.5$. Finally, we compare the first and second order result as a function of $\log(D/\omega_{\text{ph}})$ in Fig. 11. Different values for μ_c were used in the first and second order calculations, and chosen such that both calculations gave the same μ_c^* for $D/\omega_{\text{ph}} = 10$. It is quite interesting that μ_c^* then decreases in a very similar way in the two cases.

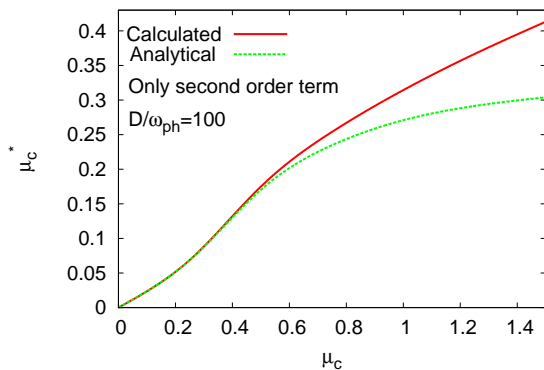


FIG. 10: (Color online) μ_c^* as a function of μ_c for $D/\omega_{\text{ph}} = 100$ and $\beta\omega_{\text{ph}} = 240$. The figure shows the calculated value using just the second order result for $\Gamma^{(\text{PP})}$ as well as the analytical approximation in Eq. (73).

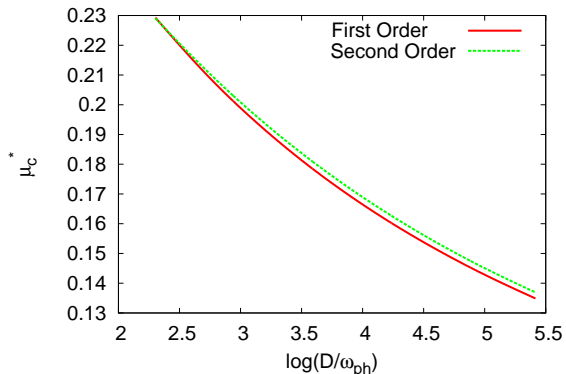


FIG. 11: (Color online) μ_c^* as a function of $\log(D/\omega_{\text{ph}})$ for $\beta\omega_{\text{ph}} = 240$ according to a first ($\mu_{c1} = 0.5$) and second ($\mu_{c2} = 0.2756$) order calculation. μ_{c1} and μ_{c2} were chosen so that the same μ_c^* was obtained in the two calculations for $D/\omega_{\text{ph}} = 10$.

We are now in the position to discuss the results for μ_c^* . We have performed calculations using the first or second order expression for $\Gamma^{(\text{PP})}$. We then either calculated Eq. (62) numerically, without any further approximations. Alternatively, we performed analytical calculations involving the neglect of additional higher order terms in U .

When the first order result for $\Gamma^{(\text{PP})}$ is used, the analytical calculations can be performed without further approximations. This leads to the Morel-Anderson result, which has two important features. When $D/\omega_{\text{ph}} \rightarrow \infty$, $\mu_c^* \rightarrow 0$, and when $U \rightarrow \infty$, $\mu_c^* \rightarrow 1/\log(D/\omega_{\text{ph}})$ stays finite and saturates. Is this still true when the second order contribution to $\Gamma^{(\text{PP})}$ is included?

The analytical results in Eqs. (72,73) have these properties. However, these results were not derived but are ansätze inspired by the Morel-Anderson result and adjusted so that they agree with the analytical calculations to low order in U . Actually, Figs. 9,10 show that although

retardation effects strongly reduce μ_c^* , there is no sign that the values saturate as U becomes very large. In this sense there is an important difference from the Morel-Anderson result. For these large values of U , higher order effects in $\Gamma^{(\text{PP})}$ become important, and it is not clear how these influence the conclusions.

The second issue is how μ_c^* is influenced when D/ω_{ph} becomes very large. As is clear from Eqs. (72,73), retardation effects also reduce the second order contribution to μ_c^* . This is also seen in Fig. 11. However, the effective band width is smaller due to the frequency dependence of the second order contribution and retardation effects are less efficient. Nevertheless, the second order contribution goes to zero as $D/\omega_{\text{ph}} \rightarrow \infty$. In this context Fig. 11 may seem surprising. One might have expected the second order contribution to drop more slowly with D/ω_{ph} . To understand this one can study Eqs. (72,73) and find the μ_{c1} and μ_{c2} which lead to the same μ_c^* in the first and second order calculation. Because of the less efficient retardation effects for the second order term, μ_{c2} has to be chosen smaller than would otherwise have been the case. The criteria for the choice of μ_{c2} is, however, independent of D . Thus the two curves in Fig. 11 should be identical according to Eqs. (72,73). The small deviation is due to the inaccuracies of these analytical results for finite U . Fig. 11, nevertheless, nicely illustrates how both the first and second order contributions are systematically reduced as D/ω_{ph} is increased.

B. Calculations for the gap at $T = 0$

In this section we conduct a complimentary analysis to extract results for μ_c^* . We calculate the spectral gap of the superconductor Δ_{sp} at $T = 0$, and show how μ_c^* enters naturally in the analytical description. We present this analysis to order U^2 . The approach here is similar to the original work by Morel and Anderson,¹⁷ which included only the first order term in U and was carried out in the $T = 0$ formalism. Here, we work on the imaginary axis in the limit $T \rightarrow 0$. Starting point is the self-consistency equation for the off-diagonal self-energy,

$$\Sigma_{21}(i\omega_n) = \frac{1}{\beta} \sum_m G_{21}(i\omega_m) K(i\omega_n, i\omega_m), \quad (74)$$

where the kernel $K(i\omega_n, i\omega_m)$ includes the following terms,

$$K(i\omega_n, i\omega_m) = g^2 D(i\omega_n - i\omega_m) + U - U^2 \Pi(i\omega_n + i\omega_m). \quad (75)$$

The second and the third term are as given in Eq. (49) and Eq. (58). The expression for $G_{21}(i\omega_m)$ was given in Eq. (15) and a semi-elliptic DOS is used in the following. We do not consider vertex corrections of the electron-phonon vertex here, and we simply use the form,

$$g^2 D(i\omega_n) = -\frac{\lambda}{\rho_0} \frac{1}{1 + (\frac{\omega_n}{\omega_{\text{ph}}})^2}. \quad (76)$$

The effect of the diagonal self-energy is taken into account in the analytical calculations for completeness with a Z -factor for small frequencies, $|\omega_n| < \omega_{\text{ph}}$. In the numerical calculations in this section it is neglected.

The self-consistency equation (74) can be solved numerically by iteration to find a solution for $\Sigma_{21}(i\omega_n)$. For an analytical solution, we need to make some approximations. At half filling we use for the Green's function for $|\omega_n| < \omega_{\text{ph}}$,

$$G_{21}(i\omega_n) \simeq -\frac{1}{t} \frac{\Sigma_{21}(i\omega_n)}{\sqrt{Z^2\omega_n^2 + \Sigma_{21}(i\omega_n)^2}} \quad (77)$$

for $\omega_{\text{ph}} < |\omega_n| < D$,

$$G_{21}(i\omega_n) \simeq -\frac{1}{t} \frac{\Sigma_{21}(i\omega_n)}{|\omega_n|} \quad (78)$$

and for $|\omega_n| > D$

$$G_{21}(i\omega_n) \simeq -\frac{\Sigma_{21}(i\omega_n)}{\omega_n^2} \simeq 0. \quad (79)$$

As discussed, $\Pi(i\omega)$ is well approximated by the form given in Eq. (33). As noted by Morel and Anderson¹⁷ the ω -dependence of the off-diagonal self-energy is very similar to the one of the pairing kernel $K(i\omega_n, i\omega_m)$. Hence, a suitable ansatz for the off-diagonal self-energy is,

$$\Sigma_{21}(i\omega) = \Delta_3 + \frac{\Delta_2}{1 + b_1|\omega| + b_2\omega^2} + \frac{\Delta_1 - \Delta_2 - \Delta_3}{1 + \left(\frac{\omega}{\omega_{\text{ph}}}\right)^2}. \quad (80)$$

It contains the parameters Δ_i . We assume that b_1 and b_2 take the same values as what is found for $\Pi(i\omega)$ in Eq. (33). By comparing the ω -dependence with the full numerical solution we find reasonable accuracy for this assumption. In general we have to solve then for the parameters three Δ_1 , Δ_2 , and Δ_3 by evaluating the self-consistency equation at suitable values of $i\omega$. Unfortunately, the general case is algebraically very involved. It will be discussed to some detail in the appendix. Here we only treat the first and purely second order cases to see the major effects.

For the first order case, we set $\Delta_2 = 0$ and omit the U^2 -term in Eq. (75). We use the self-consistency equations $\Sigma_{21}(0) = \Delta_1$, and $\Sigma_{21}(iD) \simeq \Delta_3$. When evaluating the $\Sigma_{21}(0)$ and $\Sigma_{21}(iD)$ according to Eq. (74), we approximate the integrals in order to find an analytic solution (see appendix). We also assume $\Delta_i \ll \omega_{\text{ph}} \ll D$ for simplification. Then for a self-consistent solution the parameters Δ_1 and Δ_3 have to satisfy the equations

$$\begin{aligned} \Delta_1 &= \frac{\lambda - \mu_c}{Z} \Delta_1 \log\left(\frac{2Z\omega_{\text{ph}}}{\Delta_1}\right) + a_0\lambda\Delta_3 - \mu_c\Delta_3 \log\left(\frac{D}{\omega_{\text{ph}}}\right), \\ \Delta_3 &= -\mu_c \left[\frac{\Delta_1}{Z} \log\left(\frac{2Z\omega_{\text{ph}}}{\Delta_1}\right) + \Delta_3 \log\left(\frac{D}{\omega_{\text{ph}}}\right) \right]. \end{aligned} \quad (81)$$

The coefficient a_0 is given in the appendix. This yields the non-trivial solutions

$$\Delta_1 = 2Z\omega_{\text{ph}} e^{-\frac{Z}{\lambda - \mu_c^*(1+a_0\lambda)}}, \quad \Delta_3 = -\frac{2Z\omega_{\text{ph}}\mu_c^*}{\lambda - \mu_c^*} e^{-\frac{Z}{\lambda - \mu_c^*(1+a_0\lambda)}}, \quad (82)$$

where the standard result for μ_c^* is obtained,

$$\mu_c^* = \frac{\mu_c}{1 + \mu_c \log\left(\frac{D}{\omega_{\text{ph}}}\right)}. \quad (83)$$

Note that the gap in the spectral function Δ_{sp} , found from the pole of the Green's function, occurs at $|\omega| = \Delta_1/Z$ in this approximation.

Accounting for the approximations made in this derivation we can use this form with three fitting parameters as in Eq. (27),⁵³

$$\Delta_{\text{sp}} = c_1\omega_{\text{ph}} e^{-\frac{Zc_2}{\lambda - \mu_c^*(1+c_3\lambda)}}, \quad (84)$$

where $c_1 > 0$, $c_2 > 1$. We can determine the parameters c_1 , c_2 by fitting to the numerical solution of Eq. (74) for $\mu_c = 0$ in the regime $0 < \lambda < 0.5$. Note that in contrast to the analytical solution the result of the numerical solution depends in general on the bandwidth W . It only becomes independent in the large bandwidth limit.⁵⁸

For $\mu_c = 0$, $D = 8/\omega_{\text{ph}} = 80$, we find with $c_1 = 1.7$, $c_2 = 1.07$ good agreement of the formula (84) with the numerical results for $\lambda < 0.5$ as can be seen in Fig. 12. Note that for the Holstein model and larger values of λ , the result in Eq. (84) underestimates Δ_{sp} as already pointed out by Allen and Dynes.⁵⁴

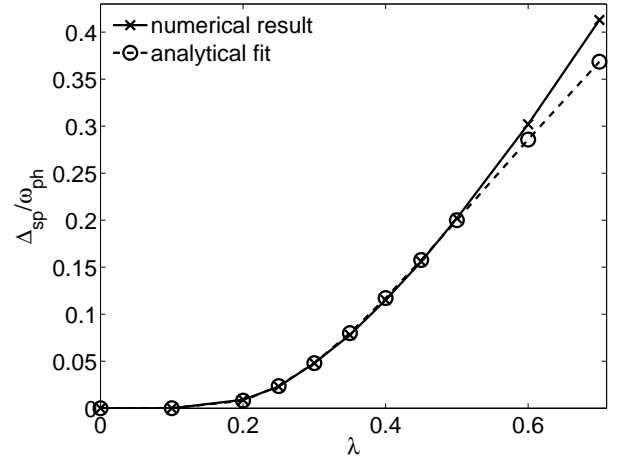


FIG. 12: The spectral gap Δ_{sp} as calculated from the numerical solution of Eq. (74) as a function of λ for $D/\omega_{\text{ph}} = 80$ in comparison with the analytical form in Eq. (84) with the parameters $c_1 = 1.7$, $c_2 = 1.07$.

For fixed $\lambda = 0.5$, we also compare the μ_c -dependence of the analytical result in Eq. (84) with the full numerical solution. In Fig. 13 a comparison can be found, where we used the same values for c_1 and c_2 as for $\mu_c = 0$ and found that $c_3 = 0.8$ gives a reasonable fit.

We analyze the situation including only the U^2 -term now. We set $\Delta_3 = 0$ in this case and omit the constant U -term in Eq. (75). To determine the parameters Δ_1 and Δ_2 , we use the following two conditions: $\Sigma_{21}(0) = \Delta_1 = \sum_i N_{1i}\Delta_i$, and $\Sigma_{21}(iD) + \Sigma_{21}(-iD) \simeq$

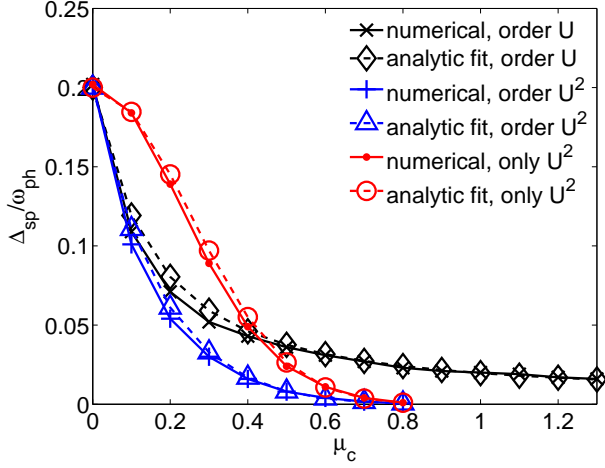


FIG. 13: (Color online) The spectral gap Δ_{sp} as calculated from the numerical solution of Eq. (74) with different kernels as a function of μ_c for $D/\omega_{\text{ph}} = 80$ in comparison with the analytical result in Eq. (84).

$2\Delta_2/(1 + b_1D + b_2D^2) = \sum_i N_{2i}\Delta_i$. This yields the self-consistency equation,

$$1 = N_{11} + \frac{N_{12}N_{21}}{1 + b_1D + b_2D^2 - N_{22}}. \quad (85)$$

Making similar approximation as in the first order calculation we find for the coefficients N_{ij} ,

$$N_{11} = \frac{1}{Z}(\lambda - a\mu_c^2) \log(T_1), \quad (86)$$

and

$$N_{21} = -\frac{2}{Z} \frac{a\mu_c^2}{1 + b_1D + b_2D^2} \log(T_1). \quad (87)$$

with

$$T_1 = \frac{Z\omega_{\text{ph}} + \sqrt{(Z\omega_{\text{ph}})^2 + \Delta_1^2}}{\Delta_1}. \quad (88)$$

One also finds

$$N_{12} = a_{12}\lambda - a\mu_c^2 \log\left(\frac{D}{\omega_{\text{ph}}}\bar{A}_{12}\right), \quad (89)$$

and

$$N_{22} = -a\mu_c^2 \frac{2}{1 + b_1D + b_2D^2} \log\left(\frac{D}{\omega_{\text{ph}}}\bar{A}_{22}\right). \quad (90)$$

The expressions for a_{12} , \bar{A}_{12} and for \bar{A}_{22} can be found in the appendix. The coefficients $\bar{A}_{12} < 1$ and $\bar{A}_{22} < 1$ appear due to additional terms to $1/\omega$ in the integrand which accelerate the decay towards higher energy. Hence, they lead to a reduced effective bandwidth, $D \rightarrow \bar{A}_{22}D$ as discussed in the previous section. The solution of Eq. (85) yields

$$\Delta_1 = 2Z\omega_{\text{ph}}e^{-\frac{Z}{\lambda - \mu_c^*(1 + a_{12}\lambda) - \mu_{c,1}^*}}, \quad (91)$$

with

$$\mu_c^* = \frac{a\mu_c^2}{1 + a\mu_c^2 \log\left(\frac{D}{\omega_{\text{ph}}}\bar{A}_{22}\right)}, \quad (92)$$

and

$$\mu_{c,1}^* = \frac{\log\left(\frac{\bar{A}_{22}}{\bar{A}_{12}}\right)a^2\mu_c^4}{1 + a\mu_c^2 \log\left(\frac{D}{\omega_{\text{ph}}}\bar{A}_{22}\right)}. \quad (93)$$

The result for μ_c^* has the same form as what was derived in Eq. (73). In addition a higher order term $\mu_{c,1}^*$ appears. In the first order calculations all higher order contributions cancel in the numerator of the expression for μ_c^* . However, in the second order calculation this is not the case anymore and an additional term remains. The coefficient $\log(\bar{A}_{22}/\bar{A}_{12})$ does not increase with the bandwidth W and therefore the whole term becomes small in the large bandwidth limit due to the logarithm in the denominator. For the relevant values one has $\bar{A}_{22}/\bar{A}_{12} \approx 2$ such that the coefficient of the μ_c^2 is relatively small and the term does not contribute much for small values of μ_c . For larger values, however, it does play a role. Thus it can account for the discrepancy between the numerical and the analytical result from Eq. (73) observed in Fig. 10, where the numerical result does not seem to saturate.

We would like to check these analytical findings with the full numerical solution of the self-consistency equation. Formally, we had found very similar results to the ones of the last section derived from the projection scheme. For the comparison with the numerics we take these expressions and use the values for the parameters derived there, i.e. we use $\bar{A}_{22} \rightarrow A_2$, where $A_2 = 0.197$ or $\log(A_{22}) = -1.624$. We omit the term $\mu_{c,1}^*$, and for c_1 , c_2 we take the same values as above, and we use $a_{12} = c_3$. The reason for this procedure is that due to a number of approximations involved in the analytic calculation the results for these coefficient do not tend to be very accurate. Moreover, we aim for a unified description with as little parameters as possible.

The result for the “only U^2 ”-calculation is added in Fig. 13 and compared with the full numerical solution. We find good agreement. For small values of μ_c the reduction of Δ_{sp} is smaller than for the first order term, but then Δ_{sp} drops more rapidly. Notice that the second order result for μ_c^* is analogous in the form to the first order calculation. The difference is the factor $\bar{A}_{22} < 1$ in the logarithm in the denominator. Hence, the retardation effects are less effective in this case as discussed in the previous section. The results here are derived independently from the arguments of the last section, but are fully consistent with them. The higher order term $\mu_{c,1}^*$ is not very important for the values of μ_c appearing in Fig. 13.

In the general case including both the first and second order terms in Eq. (75), we have to solve for three parameters and hence have three self-consistency equations to be solved. In general this can be written as a matrix

equation $\Delta = \underline{M}\Delta$. Algebraically this becomes rather lengthy and yields a number of different terms for μ_c^* , as discussed in the appendix. To simplify the discussion, we use results in the form of Eq. (84) with μ_c^* as introduced in Eq. (72),

$$\mu_c^* = \frac{\mu_c + a\mu_c^2}{1 + \mu_c \log\left(\frac{D}{\omega_{\text{ph}}}\right) + a\mu_c^2 \log\left(\frac{D}{\omega_{\text{ph}}} A_{22}\right)}, \quad (94)$$

for comparison with the numerical results. In Fig. 13 we have included the numerical result of Eq. (74) with the full kernel in Eq. (75). We also included the analytical description based on Eq. (84) and (72) with the same value $\log(A_{22}) = -2.28$ or $A_{22} = 0.1022$ as in the previous section. We find a rather good agreement for the range of values of μ_c .

We can accurately calculate the dependence of the spectral gap Δ_{sp} on μ_c for given λ , D and ω_{ph} numerically. However, it is not possible to calculate μ_c^* directly from the self-consistency equation (74). If we assume that the form of Eq. (84), which neglects higher order terms of the form Eq. (93), gives a good description and we can solve for μ_c^* ,

$$\mu_c^* = \frac{\lambda}{1 + c_3\lambda} + \frac{Zc_2}{\log\left(\frac{\Delta_{\text{sp}}}{c_1\omega_{\text{ph}}}\right)(1 + c_3\lambda)}. \quad (95)$$

As higher order terms are neglected this is not the complete result for μ_c^* for the whole range of μ_c . However, if μ_c^* is interpreted as the quantity in competition with λ to cause superconductivity, then this form is useful and the inversion of Eq. (84) can give us an estimate for μ_c^* .

The results for μ_c^* obtained from Eq. (95) together with the analytical estimates in Eqs. (1,73,72) can be found in Fig. 14.

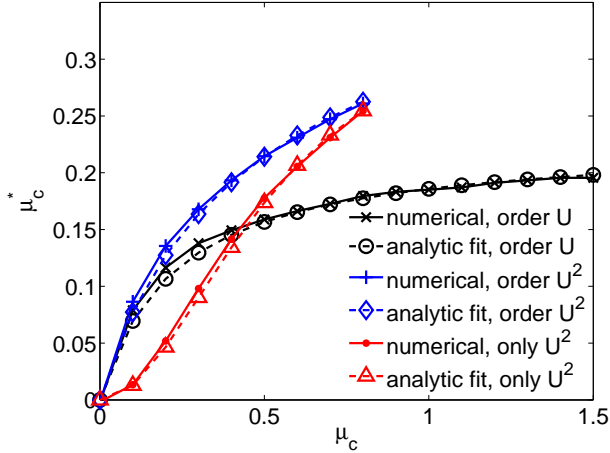


FIG. 14: (Color online) μ_c^* as a function of μ_c for $D/\omega_{\text{ph}} = 80$ computed from Eq. (95). We show in comparison the result for the first order and the second order calculation. The fit parameters are c_1 , c_2 and c_3 are the same as above.

The results look very similar to the ones in the previous section in Fig. 9. For small μ_c , μ_c^* increases linearly

with μ_c in Eqs. (1,72). This implies an initially relatively large drop of superconductivity once the Coulomb repulsion becomes finite (see Fig. 13). However, then the curves bend and the analytical results saturate. Only for very small values of μ_c the first and second order results are in agreement, otherwise the second order result is substantially larger. For the first order calculation the upper boundary is given by $\mu_{c,\text{max}}^* = 1/\log(\frac{D}{\omega_{\text{ph}}})$ independent of μ_c . It is reached both in the limit of large μ_c and large ratio D/ω_{ph} . For instance for $D/\omega_{\text{ph}} = 1000$, we have $\mu_{c,\text{max}}^* \approx 0.145$, similar to what is usually used in the literature. Using $\mu_c = 0.5$ for the screened Coulomb interaction gives with the same ratio for D/ω_{ph} the value $\mu_c^* = 0.112$ (see Tab. I).

D/ω_{ph}	10	100	1000
μ_c^* in Eq. (1)	0.232	0.151	0.112
$\bar{\mu}_c^*$ in Eq. (44)	0.286	0.172	0.123
μ_c^* in Eq. (72)	0.386	0.204	0.139

TABLE I: Exemplary values for μ_c^* for $\mu_c = 0.5$.

D/ω_{ph}	10	100	1000
μ_c^* in Eq. (1)	0.303	0.172	0.127
$\bar{\mu}_c^*$ in Eq. (44)	0.366	0.199	0.136
μ_c^* in Eq. (72)	0.700	0.268	0.166

TABLE II: Exemplary values for μ_c^* for $\mu_c = 1$.

We can see that the higher order results for μ_c^* are generally substantially larger than in the first order calculation. In particular the results are larger than the simple minded estimate, $\bar{\mu}_c^*$ in Eq. (44), where retardation effects are the same for the first and second order term. For this expression the limits of large bandwidth and large μ_c lead to the same result $\bar{\mu}_{c,\text{max}}^* = 1/\log(\frac{D}{\omega_{\text{ph}}})$, which is however reached already for smaller values, e.g. for $\mu_c = 0.5$ we have $\bar{\mu}_c^* = 0.1233$. In contrast, the result in Eq. (72) goes to $\mu_{c,\text{max}}^* = 1/\log(\frac{D}{\omega_{\text{ph}}} A_{22})$ in the limit of large μ_c and to $\mu_{c,\text{max}}^* = 1/\log(\frac{D}{\omega_{\text{ph}}})$ in the limit of a very large bandwidth. With the estimate for A_{22} above we find for $D/\omega_{\text{ph}} = 1000$ that in the large μ_c limit $\mu_{c,\text{max}}^* \approx 0.216$ is about 50 % larger than the first order estimate. For comparison we give some results in tables I and II for $\mu_c = 0.5$, $\mu_c = 1$, and the ratios $D/\omega_{\text{ph}} = 10, 100, 1000$. Notice, that the more accurate result for μ_c^* as obtained from the numerical calculation and shown in Fig. 9 can be still significantly larger than the estimate in Eq. (72). We conclude that the usual result in Eq. (1) substantially underestimates μ_c^* for intermediate and larger values of μ_c . However, for very large values of D/ω_{ph} retardation effects are operative in all cases and lead to a strongly reduced value of μ_c^* .

C. Calculations for T_c

For completeness we also include a brief section on the critical temperature T_c . It is analyzed similar to the last section. The basis for the calculations is the pairing matrix in Eq. (13). For the pairing vertex we use the same terms as in the previous section in Eq. (75),

$$\Gamma^{(\text{pp})}(i\omega_{n_1}, i\omega_{n_2}; 0) = -K(i\omega_{n_1}, i\omega_{n_2}). \quad (96)$$

The effect of the Z -factor is neglected. Then with the bare Green's function and a semi-elliptic DOS

$$\tilde{\chi}^0(i\omega_{n_1}; 0, 0) = -\frac{G(i\omega_{n_1})}{i\omega_{n_1}} = \rho_0 \frac{\pi}{2t} \left(\sqrt{1 + \frac{4t^2}{\omega_n^2}} - 1 \right). \quad (97)$$

$\Pi(i\omega_n)$ is calculated numerically from the free Green's function. With this we compute the matrix M_{n_1, n_2} in Eq. (13) and search for the largest eigenvalue. We compare the results for T_c for three different calculations: (1) including only the U -term, (2) including only the U^2 -term and (3) including both.

Apart from the first order calculation it is not easy to find a good analytic approximation for the eigenvalue equation (12). In principle, one can do something similar to what has been done in the last section and make an appropriate ansatz for the eigenvector. To first order in U this works reasonably well. We find a result of the standard form,

$$T_c = c_1 \omega_{\text{ph}} e^{-\frac{Zc_2}{\lambda - \mu_c^*(1+c_3\lambda)}}. \quad (98)$$

where μ_c^* is given by Eq. (83). For the higher order analysis we did not pursue an analytical solution, and instead also assume T_c as in Eq. (98) and for μ_c^* the form in Eq. (72).

First we fix the constants c_1 and c_2 by fitting to the result for $\mu_c = 0$, see Fig. 15. We take the value $c_1 = 1/1.2 \approx 0.833$ as in Ref. 54 and find a good fit for $c_2 = 1.04$. Similar as before the agreement is only good up to values of $\lambda < 0.5$.

In Fig. 16 we give the numerical result for T_c as a function of μ_c for the first order calculation, only the second order and first plus second order. We have kept $\lambda = 0.5$ constant.

T_c decays in a very similar way as the spectral gap when μ_c is increased. We included results from the analytic fit form in Eq. (98) with the value $c_3 = 0.8$. For the first order calculation, we find good agreement with the numerical result for the case $\lambda = 0.5$. For the second order results we use the same parameters as before and the fits are reasonable, i.e. they show that the functional form is close to the actual result.

Note, that in spite of the identical form for the pairing kernel, the results for T_c here and the ones for the gap at $T = 0$ in the previous section are obtained from two independent calculations. The results indicate that for the range of parameters studied the analytical expressions

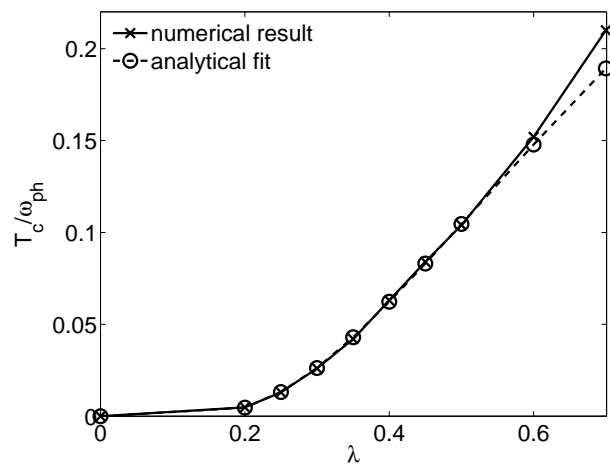


FIG. 15: (Color online) T_c as a function of λ for $D/\omega_{\text{ph}} = 80$.

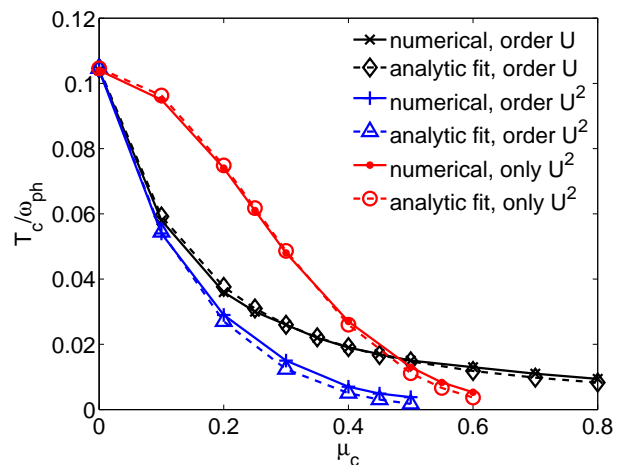


FIG. 16: (Color online) T_c as a function of μ_c for $D/\omega_{\text{ph}} = 80$.

Eqs. (1,73,72) describe the effect of μ_c^* on T_c quite accurately. In particular the results are very similar to what has been found in the projective approach before, and hence a consistent picture emerges. We conclude that higher order dynamic effects, and in particular the second order contributions, give an important correction to the usual results for the Coulomb pseudopotential. Not only does the higher order term give a direct increase of the coupling, as would be the case in expression in Eq. (44) it also leads to a reduced effective bandwidth in the logarithm in the denominator. This is an effect which to our knowledge has not been discussed in the literature so far. In the following section we analyze how these effects are manifest in the non-perturbative DMFT calculations.

VI. DMFT AND PERTURBATIVE RESULTS

In this section we put the analysis of the previous sections together and compare with non-perturbative

DMFT calculations, which include all possible renormalization effects. We first clarify that it is therefore very important to work with renormalized parameters for the interpretation of the results. Then we demonstrate up to which interaction strengths the perturbative results derived in the previous section are reliable.

We focus on calculations for the spectral gap Δ_{sp} at $T = 0$ and consider a half filled band. The spectral gap Δ_{sp} is extracted directly from the gap edges of the diagonal spectral function. It is usually well approximated by the product $z\Sigma_{21}(0)$, but it can be a bit larger due to the frequency dependence of the off-diagonal self-energy. For an interpretation of the DMFT results we need to compare with the perturbation theory (PT) results. We include the following terms for the self-consistent PT calculation: For the diagonal and off-diagonal self-energy we use Eqs. (51) and (53). The vertex is approximated by the contributions from RPA screening in Eq. (34) up to second order in U and the second order in U corrections in Fig. 5. For a small phonon frequency, the $\omega = 0$ value of the vertex function provides a good approximation. From the diagrams in U we take Eqs. (49), and (54)-(57) into account. The phonon propagator is taken as an input from DMFT calculations and not calculated self-consistently, similar to what has been done in Ref. 13.

To get a feeling for the renormalization effects let us first consider calculations, where the bare parameters $\lambda_0 = \rho_0 2g^2/\omega_0$ and ω_0 in the Hamiltonian (2) are kept fixed. For $\mu_c = 0$ the system has a superconducting solution and we analyze how the gap Δ_{sp} is affected, when μ_c becomes finite. For $\lambda_0 = 0.308$ and $\lambda_0 = 0.382$, the corresponding spectral gaps Δ_{sp} are shown in Fig. 17. For comparison we have also included the results from the self-consistent PT as explained above in Fig. 17. These are seen to be in very good agreement with the DMFT result.

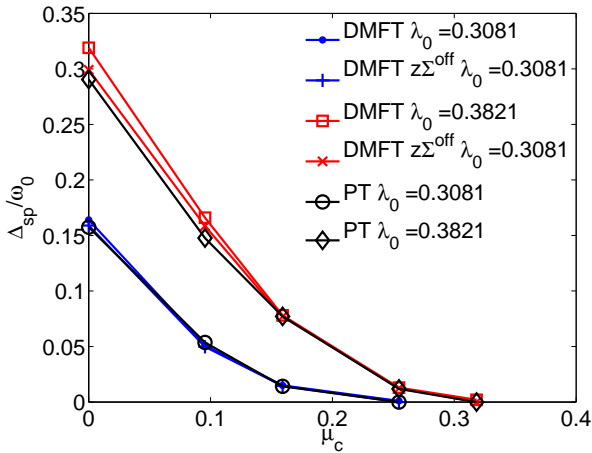


FIG. 17: (Color online) Behavior of the spectral gap Δ_{sp} and $z\Sigma^{\text{off}}(0)$ for constant $\lambda_0 = 0.308$ and $\lambda_0 = 0.382$ ($\omega_0 = 0.1$ in both cases) as a function of μ_c .

We find a rapid decrease of Δ_{sp} when μ_c becomes finite,

similar to the results in Fig. 13. However, notice that Δ_{sp} goes to zero for even smaller values of $\mu_c \sim 0.3$. Naively one could conclude that μ_c^* is even larger than what was discussed in the last section even though we are still at very weak coupling in U . As we will see, however, this drastic reduction of Δ_{sp} has a different origin. It can be understood by analyzing the relevant effective parameters and the PT results.

Since, as shown in Sec. V many aspects of the PT are well described by approximate analytical results, such as Eq. (72) for μ_c^* or Eq. (84) for Δ_{sp} , it makes sense to use those equations to analyze the results. In Sec. V the equations were used in terms of bare parameters, but to understand the DMFT results we need to use renormalized parameters. Those effective parameters extracted from the DMFT calculation are shown in Fig. 18 as function of μ_c .

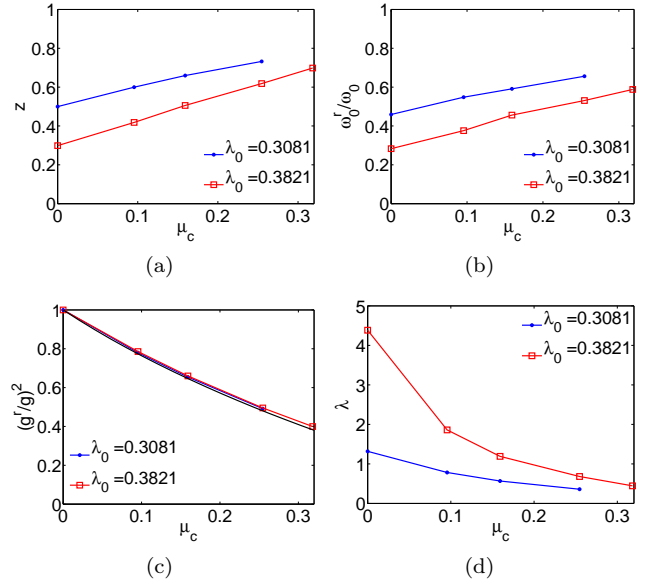


FIG. 18: (Color online) The effective parameters (a) the quasiparticle renormalization z , (b) the renormalized phonon frequency ω_0^r/ω_0 (c) the renormalized coupling constant $(g^r/g)^2$ (the full line corresponds to the result with a and b obtained from the free Green's functions) and (d) the effective λ as a function of μ_c .

The z -factor in Fig. 18 (a) increases moderately with μ_c . According to Eq. (84) with $Z = z^{-1}$ this would actually help superconductivity, so it can not be responsible for the reduction in Fig. 17. The renormalized phonon frequency ω_0^r in Fig. 18 (b) also increases with μ_c showing that corrections to the phonon self-energy and electron-phonon vertex from finite U are important. In the prefactor of Eq. (84) with $\omega_{\text{ph}} = \omega_0^r$ this leads to an enhancement of Δ_{sp} , whereas μ_c^* increases with ω_0^r which leads to a reduction of Δ_{sp} . Both effects are not strong enough to be decisive. The strongest and most important effect of μ_c can be seen in Fig. 18 (c) and (d), where we plot the renormalized coupling g^r from Eq. (39) and

the effective λ according to Eq. (29). The parameters a and b in Eq. (39) are calculated from the full Green's functions. We find that the renormalized coupling g^r decreases substantially with μ_c . In addition the phonon self-energy is modified for finite U . Therefore, the effective λ becomes much smaller. So the main reason for the rapid suppression of Δ_{sp} is the strong effect of the corrections to the electron-phonon vertex and to the phonon self-energy, such that the effective λ decreases.

Using values $\omega_{\text{ph}} = \omega_0^r$ we can calculate results for the Coulomb pseudopotential μ_c^* according to Eq. (72). The ratio of electron over phonon scale is with $D/\omega_0^r \sim 35$ not as large as in the last section, and thus retardation effects not as effective. For the largest value $\mu_c \simeq 0.318$ we find $\mu_c^* \simeq 0.2$. At this μ_c we have $\lambda \simeq 0.45$ and the analytic expression in Eq. (84) yields $\Delta_{\text{sp}}/\omega_0 \simeq 0.0002$, where $Z = z^{-1}$, $\omega_{\text{ph}} = \omega_0^r$, and for the fitting parameters c_i take the same values as in Sec. V B. This is in agreement with the DMFT finding that superconductivity goes to zero then. If we compare the results for the spectral gap according to Eq. (84) with the renormalized parameters in Fig. 18 with the results from the full calculation in Fig. 17 we find good agreement. Hence we conclude that the superconducting state at small μ_c can be well understood in terms of the effective parameters λ , ω_0^r , z and μ_c^* and the approximate equations for μ_c^* and Δ_{sp} .

The conclusion up to this stage is that the strongest effect of the Coulomb repulsion in the DMFT calculations is to renormalize the effective λ via electron-phonon vertex and phonon propagator such that superconductivity drops to zero rapidly. Even at very weak coupling these effects play an important role in the Hubbard-Holstein model and must be taken into account. Since in this work our main interest is the effectiveness of retardation effects visible in the direct competition between λ and μ_c^* , we will offset the vertex-correction effect in the following. We do this by appropriately adjusting the bare parameters, i.e., increasing λ_0 and ω_0 . We proceed by keeping $\lambda = \lambda(\mu_c)$ as defined in Eq. (29) constant. For g^r we rely on the perturbative results. This was found to give a relatively good description up to $U \sim W/2$.⁵⁵ First we do a calculation for certain bare values ω_0 and λ_0 at $\mu_c = 0$. From the phonon spectral function we can then extract the value ω_0^r and λ from (29) where, $g^r = g$. Then we choose a finite value of μ_c . We have to increase λ_0 and ω_0 , such that ω_0^r roughly equals the $U = 0$ value and λ remains approximately the same according to Eq. (29). For the renormalized coupling g^r entering Eq. (29) we consider two conditions: (a) the second order expansion as in Eq. (41) and (b) the RPA series plus the second order terms as in Eq. (39). With the set of bare parameters $(\lambda_0, \omega_0, \mu_c)$ found from this procedure we also do perturbative calculations for comparison. We distinguish PT-a, which includes up to second order diagrams for the electron-phonon vertex, and PT-b which includes the RPA series plus the second order terms for the electron-phonon vertex. The results of such a calculation, where $\lambda \simeq 1$ according to condition (a) and

$\omega_0^r/D \simeq 0.025$ are shown in Fig. 19 as Δ_{sp} vs μ_c .

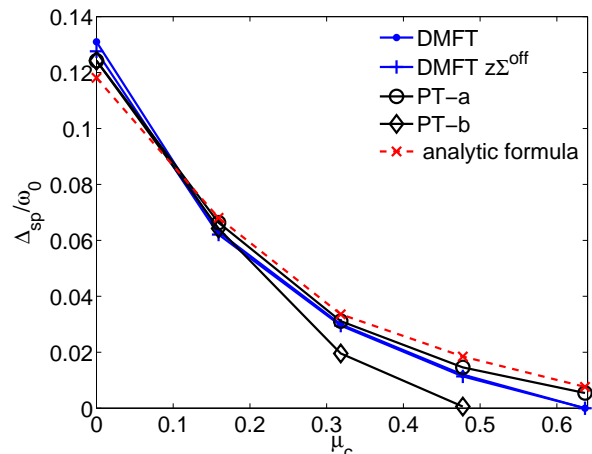


FIG. 19: (Color online) Behavior of the DMFT result for the spectral gap Δ_{sp} and $z\Sigma^{\text{off}}(0)$ for constant $\lambda \simeq 1$ according to condition (a) for the vertex corrections (see text), $\omega_0^r \simeq 0.05$ as a function of μ_c in comparison with PT-a and PT-b (see text) and the analytic formula in Eq. (84).

The DMFT results show a steady decrease of Δ_{sp} on increasing μ_c . Since the effective λ and ω_{ph} are kept constant the diminution of Δ_{sp} is now due to the competition with the Coulomb repulsion μ_c . To understand the result quantitatively we compare it with the perturbative calculations PT-a, PT-b and the analytic results based on Eq. (84) using the effective parameters and μ_c^* according to Eq. (72) with the value of A_{22} as in Sec. V. We find a relatively good agreement of the DMFT result with PT-a and the analytic formula up to $\mu_c \sim 0.5$. This demonstrates that (i) the effective parameter description is appropriate, (ii) the electron-phonon vertex correction according to condition (a) is suitable and (iii) that the derived higher order form for the Coulomb pseudopotential in Eq. (72) captures correctly the results of the PT and the of the full DMFT calculation. This validates the analysis of the Sec. V in a more complete calculation and it corroborates our findings for μ_c^* and retardation effects by comparison with non-perturbative DMFT up to intermediate values of $\mu_c \sim 0.5$. For larger values of μ_c , higher order correction enhance the value of μ_c^* such that Δ_{sp} is suppressed stronger. In addition the electron-phonon vertex is not well described by condition (a) anymore. The PT-b calculation agrees with DMFT quite well up to values $\mu_c \sim 0.3$, but then overestimates the reduction of the electron-phonon vertex and therefore leads to a too strong suppression of superconductivity.

To extend the present analysis to larger values of μ_c , one needs to find reliable estimates for the full renormalized electron-phonon vertex $\Gamma_U^{(\text{ep})}$. A higher order perturbative analysis or non-perturbative calculation for this quantity could provide this. A consistent calculation up to certain order in μ_c should then also include higher order corrections to the self-energies, which will compli-

cate the analytical calculation for μ_c^* further. This is beyond the scope of this work.

VII. CONCLUSIONS

For the occurrence of conventional superconductivity it is important that on the one hand there is a sizeable electron-phonon coupling and on the other that the detrimental effects of the Coulomb repulsion are reduced sufficiently by screening and retardation effects. We have stressed in this article that while the effect of the former can be described in a controlled fashion by Migdal-Eliashberg theory, the standard approach to the latter is based on an uncontrolled approximation, since there is no Migdal theorem for the Coulomb interaction. For the Hubbard-Holstein model we have analyzed this issue in a controlled framework by a combination of perturbative calculations and non-perturbative DMFT calculations. We have shown that the conventional arguments based on the lowest order diagrams become modified when higher order corrections are taken into account. There is still a reduction of the Coulomb repulsion due to logarithmic terms in the denominator. This demonstrates that indeed a small value of μ_c^* can be obtained due to retardation effects even when higher order corrections are considered. Thus our results support the arguments by Morel and Anderson qualitatively. However, the effective energy scale separation is reduced. This is due to the dynamic behavior of the higher order diagrams which make retardation effects less operative. This result was shown explicitly in two independent calculations in a combination of analytical and numerical arguments. By studying the occurrence of superconductivity with DMFT, where all higher order corrections are present, we were able corroborate our findings up to intermediate coupling strength. The perturbative approach allowed us to distinguish different renormalization effects. Our analysis is limited to intermediate coupling strength due to the difficulty to reliably estimate the vertex corrections to the electron-phonon vertex. Non-perturbative calculations for this quantity would be desirable.

We conclude that the usual expression for μ_c^* in Eq. (1) is only valid for small values for μ_c . The second order corrections lead to less efficient retardation effects as shown in Eq. (72),

$$\mu_c^* = \frac{\mu_c + a\mu_c^2}{1 + \mu_c \log\left(\frac{E_{el}}{\omega_{ph}}\right) + a\mu_c^2 \log\left(\alpha \frac{E_{el}}{\omega_{ph}}\right)}, \quad (99)$$

where we found $\alpha \approx 0.1$ for a typical large energy separation of electron and phonon scale E_{el}/ω_{ph} . The coefficient a is given by the limit $\omega \rightarrow 0$ of the particle-hole bubble Π divided by ρ_0 , the DOS at the Fermi energy, and α can be estimated from the decay of Π with ω . In addition higher order terms appear such that μ_c^* does not saturate in the limit of large μ_c . Thus, for systems with sizeable effective Coulomb repulsion we should expect larger values

for μ_c^* than the traditional quote $\mu_c^* \sim 0.1$. As a consequence the values for μ_c^* are not as universal as sometimes claimed and predictions for T_c can be unreliable.

It is premature to draw detailed conclusion from our calculations for real materials such as lithium, since the Hubbard model is not an accurate description for itinerant metallic systems, which are better described by an electron gas model. Nevertheless one can understand our results as a qualitative trend, which shows that for system with less efficient screening, such that μ_c is larger, we expect an enhanced value of μ_c^* as compared to what is traditionally quoted. This could be expected in systems with larger values of r_s . Hence our conclusions would seem to be line with the observation in a number of materials, such as Li with enhanced μ_c^* , and what is quoted in work based on DFT calculations.¹⁶ Similar conclusions are important for systems where the ratio E_{el}/ω_{ph} is reduced from the usual scenario, which could be the case in picene. We would like to stress, however, that a more accurate attempt of understanding the problem should also include the dynamic effect of screening the bare Coulomb repulsion in a metal, which was not taken into account explicitly. As discussed in the introduction this can lead to very small and even negative values of μ_c^* . We expect that the combination of these effects and the corrections studied here, which lead to an enhancement, will eventually lead to the physical values occurring in nature. More detailed calculations are required to fully resolve this quantitatively. As long as μ_c^* can not be estimated reliably, the predictive power of the theory of electron-phonon superconductivity is limited.

Acknowledgment

We wish to thank N. Dupuis, A.C. Hewson, P. Horsch, C. Husemann, G. Kotliar, D. Manske, F. Marsiglio, A.J. Millis, G. Sangiovanni, and R. Zeyher for helpful discussions. JB acknowledges financial support from the DFG through BA 4371/1-1, and JH acknowledges support from the grant NSF DMR-0907150.

Appendix A: Details for the calculation of the spectral gap

In this appendix we collect some details for the analytic calculation in Sec. V B.

1. Integrals for the first order case

For $\Sigma_{21}(0)$ we approximate the integrals over small frequencies,

$$\frac{1}{2\pi} \int_{-\omega_{ph}}^{\omega_{ph}} d\omega G_{21}(i\omega) g^2 D(-i\omega) \simeq \frac{\Delta_1 \lambda}{Z} \log(T_1), \quad (A1)$$

and

$$\frac{1}{2\pi} \int_{-\omega_{\text{ph}}}^{\omega_{\text{ph}}} d\omega G_{21}(i\omega)U = \frac{\Delta_1 \mu_c}{Z} \log(T_1), \quad (\text{A2})$$

where T_1 is given in (88). For larger frequencies we write

$$\frac{1}{2\pi} \left[\int_{-D}^{-\omega_{\text{ph}}} d\omega + \int_{\omega_{\text{ph}}}^D d\omega \right] G_{21}(i\omega)g^2 D(-i\omega) = a_0 \Delta_3 \lambda, \quad (\text{A3})$$

and

$$\frac{1}{2\pi} \left[\int_{-D}^{-\omega_{\text{ph}}} d\omega + \int_{\omega_{\text{ph}}}^D d\omega \right] G_{21}(i\omega)U = -\Delta_3 \mu_c \log\left(\frac{D}{\omega_{\text{ph}}}\right). \quad (\text{A4})$$

We have

$$a_0 = \int_{\omega_{\text{ph}}}^D d\omega \frac{1}{\omega} \frac{1}{1 + \frac{\omega^2}{\omega_{\text{ph}}^2}} = \frac{1}{2} \log\left(2 \frac{D^2}{\omega_{\text{ph}}^2 + D^2}\right). \quad (\text{A5})$$

For $\Sigma_{21}(iD)$, the electron-phonon contribution is small for $\omega_{\text{ph}}/D \ll 1$, and the Coulomb contribution is the same as above. This yields Eq. (81).

2. Integrals for the only second order case

We give some results for the second order calculation. To determine the coefficient \bar{A}_{12} we calculate

$$\int_{\omega_{\text{ph}}}^D d\omega \frac{1}{\omega} \frac{1}{f_1(\omega)^2} = \log\left(\frac{D}{\omega_{\text{ph}}} \bar{A}_{12}\right), \quad (\text{A6})$$

where

$$f_1(\omega) = 1 + b_1|\omega| + b_2\omega^2. \quad (\text{A7})$$

One finds that

$$\bar{A}_{12} = \sqrt{\frac{f_1(\omega_{\text{ph}})}{f_1(D)}} \exp\left[\frac{1}{B_1^2} \left(\frac{2b_2 - (b_1^2 + b_1 b_2 D)}{f_1(D)} - \frac{2b_2 - (b_1^2 + b_1 b_2 \omega_{\text{ph}})}{f_1(\omega_{\text{ph}})} \right)\right] \exp\left(\frac{b_1^3 - 6b_1 b_2}{B_1^2} f_a\right)$$

with $B_1 = \sqrt{4b_2 - b_1^2}$ and

$$f_a = \arctan\left(\frac{b_1 + 2b_2 D}{B_1}\right) - \arctan\left(\frac{b_1 + 2b_2 \omega_{\text{ph}}}{B_1}\right). \quad (\text{A8})$$

By comparing the integrals in Eq. (A4) and Eq. (A6) we see that the factor $0 < \bar{A}_{12} < 1$ leads to a reduction of the effective bandwidth. For the given fitting values b_1 , b_2 , and large ratios $D/\omega_{\text{ph}} > 100$ one finds $\bar{A}_{12} \approx 0.2$,

which can be compared to the calculation in Eq. (71). The coefficient \bar{A}_{22} is obtained from the integral

$$\int_{\omega_{\text{ph}}}^D d\omega \frac{1}{\omega} \frac{1}{f_1(\omega)} \left(\frac{1}{f_1(D+\omega)} + \frac{1}{f_1(D-\omega)} \right) = \frac{2 \log\left(\frac{D}{\omega_{\text{ph}}} \bar{A}_{22}\right)}{f_1(D)}.$$

The integral on the left hand side can be carried out analytically, but the expression is lengthy and not instructive. We can express \bar{A}_{22} as

$$\bar{A}_{22} = \exp\left[\int_{\omega_{\text{ph}}}^D d\omega \frac{1}{\omega} \left(\frac{f_1(D)}{2f_1(\omega)} \left(\frac{1}{f_1(D+\omega)} + \frac{1}{f_1(D-\omega)} \right) - 1 \right)\right].$$

Since the function $1/f_1(D+\omega) + 1/f_1(D-\omega)$ increases in the integration interval the coefficient \bar{A}_{22} comes out larger than \bar{A}_{12} . For the parameters above we find $\bar{A}_{22} \approx 0.44$. The coefficient for λ reads

$$a_{12} = \int_{\omega_{\text{ph}}}^D d\omega \frac{1}{\omega} \frac{1}{1 + \frac{\omega^2}{\omega_{\text{ph}}^2}} \frac{1}{f_1(\omega)} \quad (\text{A9})$$

The integral can be solved analytically but the expression is lengthy. Due to the reduction factor $1/f_1(\omega)$, a_{12} term is a bit smaller than a_0 in Eq. (A5).

3. Calculation up to second order

We use the following three conditions: (i) $\Sigma_{21}(0) = \Delta_1$, (ii),

$$\Sigma_{21}(i\bar{b}_1) + \Sigma_{21}(-i\bar{b}_1) \simeq 2\Delta_3 + 2\Delta_2/f_1(\bar{b}_1), \quad (\text{A10})$$

with $\bar{b}_1 \equiv 1/b_1$, and (iii),

$$\Sigma_{21}(iD) + \Sigma_{21}(-iD) \simeq 2\Delta_3 + 2\Delta_2/f_1(D). \quad (\text{A11})$$

We use $\Sigma_{21}(0) = \sum_i N_{1i} \Delta_i$,

$$\Sigma_{21}(i\bar{b}_1) + \Sigma_{21}(-i\bar{b}_1) = \sum_i N_{2i} \Delta_i, \quad (\text{A12})$$

$$\Sigma_{21}(iD) + \Sigma_{21}(-iD) = \sum_i N_{3i} \Delta_i. \quad (\text{A13})$$

This implies $N_{1i} = M_{1i}$,

$$M_{21} = f_1(\bar{b}_1) N_{21}/2, M_{22} = f_1(\bar{b}_1) N_{22}/2, \quad (\text{A14})$$

$$M_{23} = f_1(\bar{b}_1) (N_{23} - 2)/2, M_{31} = N_{31}/2, \quad (\text{A15})$$

$$M_{32} = (N_{32} - 2/f_1(D))/2, M_{33} = N_{33}/2. \quad (\text{A16})$$

The calculations give with certain approximations in the integrals

$$N_{11} = \frac{1}{Z} (\lambda - \mu_c - a\mu_c^2) \log(T_1), \quad (\text{A17})$$

$$N_{12} = a_{12}\lambda - \mu_c \log\left(\frac{D}{\omega_{\text{ph}}} A_{12}^{(1)}\right) - a\mu_c^2 \log\left(\frac{D}{\omega_{\text{ph}}} A_{12}^{(2)}\right), \quad (\text{A18})$$

$$N_{13} = \frac{1}{2}\lambda - \mu_c \log\left(\frac{D}{\omega_{\text{ph}}}\right) - a\mu_c^2 \log\left(\frac{D}{\omega_{\text{ph}}} A_{13}^{(2)}\right), \quad (\text{A19})$$

$$N_{21} = \frac{2}{Z} \left(\lambda \frac{\omega_{\text{ph}}^2}{b_1^2} - \mu_c - \frac{a\mu_c^2}{f_1(\bar{b}_1)} \right) \log(T_1), \quad (\text{A20})$$

$$N_{22} = a_{22}\lambda - 2\mu_c \log\left(\frac{D}{\omega_{\text{ph}}} A_{22}^{(1)}\right) - \frac{2a\mu_c^2}{f_1(\bar{b}_1)} \log\left(\frac{D}{\omega_{\text{ph}}} A_{22}^{(2)}\right), \quad (\text{A21})$$

$$N_{23} = a_{23}\lambda - 2\mu_c \log\left(\frac{D}{\omega_{\text{ph}}}\right) - \frac{2a\mu_c^2}{f_1(\bar{b}_1)} \log\left(\frac{D}{\omega_{\text{ph}}} A_{23}^{(2)}\right), \quad (\text{A22})$$

$$N_{31} = -\frac{2}{Z} \left(\mu_c + \frac{a\mu_c^2}{f_1(D)} \right) \log(T_1), \quad (\text{A23})$$

$$N_{32} = a_{32}\lambda - 2\mu_c \log\left(\frac{D}{\omega_{\text{ph}}} A_{32}^{(1)}\right) - \frac{2a\mu_c^2}{f_1(D)} \log\left(\frac{D}{\omega_{\text{ph}}} A_{32}^{(2)}\right), \quad (\text{A24})$$

$$N_{33} = a_{33}\lambda - 2\mu_c \log\left(\frac{D}{\omega_{\text{ph}}}\right) - \frac{2a\mu_c^2}{f_1(D)} \log\left(\frac{D}{\omega_{\text{ph}}} A_{33}^{(2)}\right). \quad (\text{A25})$$

The coefficients a_{12} , $A_{12}^{(2)} = \bar{A}_{12}$ and $A_{32}^{(2)} = \bar{A}_{22}$ were given above. The others read,

$$A_{12}^{(1)} = A_{32}^{(1)} = A_{22}^{(1)} = A_{13}^{(2)} = \sqrt{\frac{f_1(\omega_{\text{ph}})}{f_1(D)}} \exp\left[\frac{b_1}{B_1} f_a\right], \quad (\text{A26})$$

$$a_{22} = \int_{\omega_{\text{ph}}}^D d\omega \frac{1}{\omega} \frac{1}{f_1(\omega)} \left(\frac{1}{1 + \frac{(b_1+\omega)^2}{\omega_{\text{ph}}^2}} + \frac{1}{1 + \frac{(b_1-\omega)^2}{\omega_{\text{ph}}^2}} \right), \quad (\text{A27})$$

$$a_{23} = \int_{\omega_{\text{ph}}}^D d\omega \frac{1}{\omega} \left(\frac{1}{1 + \frac{(b_1+\omega)^2}{\omega_{\text{ph}}^2}} + \frac{1}{1 + \frac{(b_1-\omega)^2}{\omega_{\text{ph}}^2}} \right), \quad (\text{A28})$$

$$a_{32} = \int_{\omega_{\text{ph}}}^D d\omega \frac{1}{\omega} \frac{1}{f_1(\omega)} \left(\frac{1}{1 + \frac{(D+\omega)^2}{\omega_{\text{ph}}^2}} + \frac{1}{1 + \frac{(D-\omega)^2}{\omega_{\text{ph}}^2}} \right), \quad (\text{A29})$$

$$a_{33} = \int_{\omega_{\text{ph}}}^D d\omega \frac{1}{\omega} \left(\frac{1}{1 + \frac{(D+\omega)^2}{\omega_{\text{ph}}^2}} + \frac{1}{1 + \frac{(D-\omega)^2}{\omega_{\text{ph}}^2}} \right), \quad (\text{A30})$$

$$A_{22}^{(2)} = \exp\left[\int_{\omega_{\text{ph}}}^D d\omega \frac{1}{\omega} \left(\frac{f_1(\bar{b}_1)}{2f_1(\omega)} \left(\frac{1}{f_1(\bar{b}_1+\omega)} + \frac{1}{f_1(\bar{b}_1-\omega)} \right) - 1 \right)\right], \quad (\text{A31})$$

$$A_{23}^{(2)} = \exp\left[\int_{\omega_{\text{ph}}}^D d\omega \frac{1}{\omega} \left(\frac{f_1(\bar{b}_1)}{2} \left(\frac{1}{f_1(\bar{b}_1+\omega)} + \frac{1}{f_1(\bar{b}_1-\omega)} \right) - 1 \right)\right], \quad (\text{A32})$$

$$A_{33}^{(2)} = \exp\left[\int_{\omega_{\text{ph}}}^D d\omega \frac{1}{\omega} \left(\frac{f_1(D)}{2} \left(\frac{1}{f_1(D+\omega)} + \frac{1}{f_1(D-\omega)} \right) - 1 \right)\right]. \quad (\text{A33})$$

One can give analytic expressions for the integrals, which are however, lengthy and not very instructive. For typical values for D/ω_{ph} , we have $A_{23}^{(2)} \approx 1.6$ and $A_{33}^{(2)} \approx 1.7$. All other coefficients obey $0 < A_{ij}^{(\alpha)} < 1$, leading to a reduce effective bandwidth as discussed before. The coefficients a_{ij} are small for $D/\omega_{\text{ph}} \gg 1$.

From the matrix equation $\mathbf{\Delta} = \underline{M}\mathbf{\Delta}$, we can derive the self-consistency equation,

$$1 = M_{11} + \frac{M_{13}M_{31}}{1 - M_{33}} + \left(M_{12} + \frac{M_{32}}{1 - M_{33}} \right) \frac{M_{21}(1 - M_{33}) + M_{23}M_{31}}{(1 - M_{22})(1 - M_{33}) - M_{23}M_{32}}, \quad (\text{A34})$$

or when using the expression for M_{11} with $T_1 = \frac{Z\omega_{\text{ph}} + \sqrt{(Z\omega_{\text{ph}})^2 + \Delta_1^2}}{\Delta_1}$ as in Eq. (88),

$$1 = \frac{\log(T_1)}{Z} \left[\lambda - \mu_c - a\mu_c^2 + \frac{M_{13}M_{31} \frac{Z}{\log(T_1)}}{1 - M_{33}} + \left(M_{12} + \frac{M_{32}}{1 - M_{33}} \right) \frac{Z}{\log(T_1)} \frac{M_{21}(1 - M_{33}) + M_{23}M_{31}}{(1 - M_{22})(1 - M_{33}) - M_{23}M_{32}} \right]. \quad (\text{A35})$$

When solved for gap parameter Δ_1 , the term in the square brackets is the exponent, such that terms to the right of λ contribute to the expression for the pseudopotential μ_c^* . We now would like to argue that in an expansion in μ_c the dominant term is of the form of Eq. (72). We neglect the terms involving λ in M_{ij} to simplify the arguments. We find then that $-\mu_c - a\mu_c^2$ together with $\frac{M_{13}M_{31} \frac{Z}{\log(T_1)}}{1 - M_{33}}$ gives a term of the form in Eq. (72),

$$\mu_c^* = \frac{\mu_c + a\mu_c^2}{1 + \mu_c \log\left(\frac{D}{\omega_{\text{ph}}}\right) + a\mu_c^2 \log\left(\frac{D}{\omega_{\text{ph}}}\bar{A}_{33}^{(2)}\right)}, \quad (\text{A36})$$

where

$$\bar{A}_{33}^{(2)} = \exp \left[\int_{\omega_{\text{ph}}}^D d\omega \frac{1}{\omega} \left(\frac{1}{2} \left(\frac{1}{f_1(D + \omega)} + \frac{1}{f_1(D - \omega)} \right) - 1 \right) \right]. \quad (\text{A37})$$

There are also additional terms to order μ_c^3 and μ_c^4 whose coefficients are not proportional to $\log(D/\omega_{\text{ph}})$ in the numerator (cf. discussion in Sec. V B). The denominator in

the other part, $F_2 \equiv (1 - M_{22})(1 - M_{33}) - M_{23}M_{32}$, has similar properties to the one in Eq. (A36) but contains also contributions to order μ_c^3 and μ_c^4 and terms $\sim \log(D/\omega_{\text{ph}})^2$. Due to a cancellation the lowest order term in the numerator, $M_{21}(1 - M_{33}) + M_{23}M_{31}$, is $\sim a\mu_c^2(f_1(b_1)/f_1(D) - 1)$. From the prefactor,

$$\frac{M_{12}(1 - M_{33}) + M_{32}}{1 - M_{33}} \quad (\text{A38})$$

the lowest order term is $-1/[f_1(D)(1 - M_{33})]$. This gives a contribution

$$\sim \frac{a\mu_c^2 \left(\frac{f_1(b_1)}{f_1(D)} - 1 \right)}{f_1(D)F_2}, \quad (\text{A39})$$

which is smaller compared to $a\mu_c^2$. All other terms are of the order μ_c^3 and higher. Hence, in an expansion in μ_c the term to the right in the square brackets in Eq. (A36) gives a smaller contribution to μ_c^* . This explains why the numerical results in Sec. V B were fit well by an expression involving μ_c^* of the form in Eq. (72).

-
- ¹ M. R. Norman, *Science* **332**, 196 (2011).
² A. Gurevich, *Nat. Mater.* **10**, 255 (2011).
³ P. C. Canfield, *Nat. Mater.* **10**, 259 (2011).
⁴ K. Bennemann and J. K. (editors), *Superconductivity* (Springer, Berlin, 2008).
⁵ J. Bardeen, L. Cooper, and J. Schrieffer, *Phys. Rev.* **108**, 1175 (1957).
⁶ G. M. Eliashberg, *Sov. Phys. JETP* **11**, 696 (1960).
⁷ J. P. Carbotte, *Rev. Mod. Phys.* **62**, 1027 (1990).
⁸ F. Marsiglio and J. Carbotte, in *Superconductivity (Vol 1)*, edited by K. Bennemann and J. Ketterson (Springer, Berlin, 2008).
⁹ J. R. Schrieffer, *Theory of Superconductivity* (W.A. Benjamin, Inc., New York, 1964).
¹⁰ P. B. Allen and B. Mitrovic, in *Solid State Physics (Vol 37)*, edited by H. Ehrenreich, F. Seitz, and D. Turnbull (Academic, New York, 1982).
¹¹ A. B. Migdal, *Sov. Phys. JETP* **7**, 996 (1958).
¹² E. Maksimov and D. Khomskii, in *High temperature Superconductivity*, edited by V. Ginzburg and D. Kirzhnits (Consultants Publisher, New York, 1982).
¹³ J. Bauer, J. E. Han, and O. Gunnarsson, *Phys. Rev. B* **84**, 184531 (2011).
¹⁴ W. McMillan and J. Rowell, in *Superconductivity*, edited by R. Parks (Marcel Dekker, New York, 1969).
¹⁵ S. Y. Savrasov, D. Y. Savrasov, and O. K. Andersen, *Phys. Rev. Lett.* **72**, 372 (1994).
¹⁶ S. Y. Savrasov and D. Y. Savrasov, *Phys. Rev. B* **54**, 16487 (1996).
¹⁷ P. Morel and P. W. Anderson, *Phys. Rev.* **125**, 1263 (1962).
¹⁸ N. Bogoliubov, V. Tolmachev, and D. Sirkov, in *The Theory of Superconductivity*, edited by N. Bogoliubov (Gordon and Breach, New York, 1962).
¹⁹ M. Lüdgers, M. A. L. Marques, N. N. Lathiotakis, A. Floris, G. Profeta, L. Fast, A. Continenza, S. Massidda, and E. K. U. Gross, *Phys. Rev. B* **72**, 024545 (2005).
²⁰ M. A. L. Marques, M. Lüdgers, N. N. Lathiotakis, G. Profeta, A. Floris, L. Fast, A. Continenza, E. K. U. Gross, and S. Massidda, *Phys. Rev. B* **72**, 024546 (2005).
²¹ G. Profeta, C. Franchini, N. N. Lathiotakis, A. Floris, A. Sanna, M. A. L. Marques, M. Lüdgers, S. Massidda, E. K. U. Gross, and A. Continenza, *Phys. Rev. Lett.* **96**, 047003 (2006).
²² A. Y. Liu and M. L. Cohen, *Phys. Rev. B* **44**, 9678 (1991).
²³ C. F. Richardson and N. W. Ashcroft, *Phys. Rev. B* **55**, 15130 (1997).
²⁴ T. Bazhiron, J. Noffsinger, and M. L. Cohen, *Phys. Rev. B* **84**, 125122 (2011).
²⁵ T. L. Thorp, B. B. Triplett, W. D. Brewer, M. L. Cohen, N. E. Phillips, D. A. Shirley, J. E. Templeton, R. W. Stark, and P. H. Schmidt, *J. Low Temp. Phys.* **3**, 589 (1970).
²⁶ J. Tuoriniemi, K. Juntunen-Nurmilaukas, J. Uusvuori, E. Pentti, and A. Sebedash, *Nature* **447**, 187 (2007).

- ²⁷ R. Mitsuhashi, Y. Suzuki, Y. Yamanari, H. Mitamura, T. Kambe, N. Ikeda, H. Okamoto, A. Fujiwara, M. Yamaji, N. Kawasaki, et al., *Nature* **464**, 76 (2010).
- ²⁸ A. Subedi and L. Boeri, *Phys. Rev. B* **84**, 020508 (2011).
- ²⁹ G. Giovannetti and M. Capone, *Phys. Rev. B* **83**, 134508 (2011).
- ³⁰ M. Casula, M. Calandra, G. Profeta, and F. Mauri, *Phys. Rev. Lett.* **107**, 137006 (2011).
- ³¹ W. Kohn and J. M. Luttinger, *Phys. Rev. Lett.* **15**, 524 (1965).
- ³² N. F. Berk and J. R. Schrieffer, *Phys. Rev. Lett.* **17**, 433 (1966).
- ³³ H. Rietschel and L. J. Sham, *Phys. Rev. B* **28**, 5100 (1983).
- ³⁴ M. Grabowski and L. J. Sham, *Phys. Rev. B* **29**, 6132 (1984).
- ³⁵ M. Grabowski and L. J. Sham, *Phys. Rev. B* **37**, 3726 (1988).
- ³⁶ C. A. Kukkonen and A. W. Overhauser, *Phys. Rev. B* **20**, 550 (1979).
- ³⁷ T. Büche and H. Rietschel, *Phys. Rev. B* **41**, 8691 (1990).
- ³⁸ Y. Takada, *Phys. Rev. B* **47**, 5202 (1993).
- ³⁹ J. Bauer, J. E. Han, and O. Gunnarsson, *J. Phys.: Condens. Matter* **24**, 492202 (2012).
- ⁴⁰ J. K. Freericks and M. Jarrell, *Phys. Rev. Lett.* **75**, 2570 (1995).
- ⁴¹ E. Berger, P. Valášek, and W. von der Linden, *Phys. Rev. B* **52**, 4806 (1995).
- ⁴² Y. Takada, *J. Phys. Soc. Japan* **65**, 1544 (1996).
- ⁴³ F. D. Klironomos and S.-W. Tsai, *Phys. Rev. B* **74**, 205109 (2006).
- ⁴⁴ K.-M. Tam, S.-W. Tsai, D. K. Campbell, and A. H. Castro Neto, *Phys. Rev. B* **75**, 161103 (R) (2007).
- ⁴⁵ A. Georges, G. Kotliar, W. Krauth, and M. Rozenberg, *Rev. Mod. Phys.* **68**, 13 (1996).
- ⁴⁶ A. C. Hewson and D. Meyer, *J. Phys.: Cond. Mat.* **14**, 427 (2002).
- ⁴⁷ J. Bauer, A. C. Hewson, and N. Dupuis, *Phys. Rev. B* **79**, 214518 (2009).
- ⁴⁸ K. Wilson, *Rev. Mod. Phys.* **47**, 773 (1975).
- ⁴⁹ R. Bulla, T. Costi, and T. Pruschke, *Rev. Mod. Phys.* **80**, 395 (2008).
- ⁵⁰ R. Peters, T. Pruschke, and F. B. Anders, *Phys. Rev. B* **74**, 245114 (2006).
- ⁵¹ A. Weichselbaum and J. von Delft, *Phys. Rev. Lett.* **99**, 076402 (2007).
- ⁵² F. B. Anders and A. Schiller, *Phys. Rev. Lett.* **95**, 196801 (2005).
- ⁵³ W. L. McMillan, *Phys. Rev.* **167**, 331 (1968).
- ⁵⁴ P. B. Allen and R. C. Dynes, *Phys. Rev. B* **12**, 905 (1975).
- ⁵⁵ Z. B. Huang, W. Hanke, E. Arrigoni, and D. J. Scalapino, *Phys. Rev. B* **68**, 220507 (2003).
- ⁵⁶ A. Martin-Rodero and F. Flores, *Phys. Rev. B* **45**, 13008 (1992).
- ⁵⁷ R. Shankar, *Rev. Mod. Phys.* **66**, 129 (1994).
- ⁵⁸ F. Marsiglio, *Phys. Rev. B* **42**, 2416 (1990).